Geologically constrained morphological variability and boundary effects on embayed beaches

Carlos Loureiro [a*]

Óscar Ferreira [a]

Andrew Cooper [b]

[a] CIMA, Centre for Marine and Environmental Research, Universidade do Algarve, Campus de Gambelas, Faro 8005-139, Portugal

[b] Centre for Coastal and Marine Research, School of Environmental Sciences, University of Ulster, Cromore Road, Coleraine BT52 1SA, Northern Ireland, UK

* Corresponding author

Email:carlos.loureiro@stir.ac.uk, oferreir@ualg.pt , jag.cooper@ulster.ac.uk

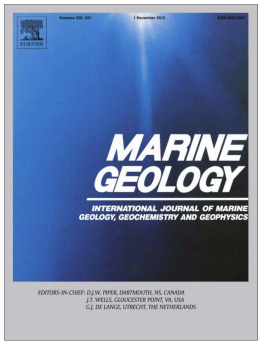

Published in:

Marine Geology

Volume 329-331, November 2012, Pages 1-15

DOI: 10.1016/j.margeo.2012.09.010

URL: https://www.sciencedirect.com/science/article/pii/S0025322712002101

Marine Geology 329–331 (2012) 1–15

Contents lists available at SciVerse ScienceDirect

Marine Geology

journal homepage: www.elsevier.com/locate/margeo

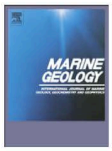

Geologically constrained morphological variability and boundary effects on embayed beaches

Carlos Loureiro [a,*], Óscar Ferreira [a], J. Andrew G. Cooper [b]

[a] CIMA, Centre for Marine and Environmental Research, Universidade do Algarve, Campus de Gambelas, Edifício 7, 8005-139 Faro, Portugal
[b] Centre for Coastal and Marine Research, School of Environmental Sciences, University of Ulster, Cromore Road, BT52 1SA, Northern Ireland, United Kingdom

ARTICLE INFO

ABSTRACT

Research Highlights

► Conspicuous alongshore variability was found in 6 embayment's from southern Portugal

► Cross- and longshore decoupling of morphological change determined by EOF analysis

► Response times increase for more constrained sites

► Increased skill of normalized wave power for morphodynamic process-response relations

► Geological boundaries considerably impact sediment transport and surfzone circulation

Geologically constrained morphological variability and boundary effects on embayed beaches

Carlos Loureiro[a,1], Óscar Ferreira[a], J. Andrew G. Cooper[b]

[a] CIMA – Centre for Marine and Environmental Research, Universidade do Algarve, Campus de Gambelas, Edifício 7, 8005-139 Faro, Portugal
cloureiro@ualg.pt; oferreir@ualg.pt

[b] Centre for Coastal and Marine Research, School of Environmental Sciences, University of Ulster, Cromore Road, BT52 1SA, Northern Ireland
jag.cooper@ulster.ac.uk

[1] Corresponding author: Telephone: +351 289800900 (ext: 7885); Fax: +351 289800969

Abstract

Headlands, rock outcrops and engineering structures impact beach and nearshore dynamics of coastal embayments, inducing boundary effects that constrain the lateral and vertical beach variability. This study analyses morphological change in six embayed beaches with diverse levels of exposure to wave action and various degrees of geological control in the mesotidal coast of southwestern Portugal. The aim is to identify whether geological boundaries constrain the morphological behaviour of embayed beaches and assess whether their effects can be decoupled from datasets of morphological change. Topographic data, obtained over a two-year period on each of the six embayments, were analysed using empirical orthogonal functions (EOF) to decompose temporal and spatial variability in the datasets. First and second mode eigenfunctions were explored using time-variable linear correlation analysis with several nearshore parameters that include hydrodynamic variables, sedimentary and geometric characteristics of each embayment in order to derive forcing-response relationships.

Our results demonstrate that natural geological boundaries constrain the morphological behaviour of embayed beaches, producing conspicuous alongshore variability in all embayments. Localized responses induced by lateral and vertical boundary interference with nearshore dynamics include beach rotation, topographically-controlled rip circulation and restrained profile fluctuation. Spatial decoupling in cross- and longshore responses is accompanied by a temporal decoupling in response times, both of which are slower in more constrained embayments (from 1 day in exposed embayments to 1 week or more in the most sheltered ones). Normalized wave power was correlated at the 99%

confidence level with the primary mode of morphological variability at most embayments, which represent 67% to 94% of the variance in the datasets. This correlation stresses the importance of combined parameterization of wave and tide forcing in process-response relations between hydrodynamics and morphological change for mesotidal coastal environments. Lateral and vertical geological boundaries exert their effects fundamentally by restraining longshore sediment transport, inducing cellular surf zone circulation and by impacting cross-shore sediment transport. It is postulated that decreasing sediment abundance and substrate depth intensify vertical boundary effects, while higher indentation and wave obliquity enhance the effects of lateral boundaries.

Keywords: coastal embayment, geological control, hard-bottom, empirical orthogonal functions, hydrodynamic forcing

1. Introduction

The presence of physical boundaries, in the form of headlands, rocky outcrops or even engineering structures, significantly impacts planform, sediment transport and morphodynamics of embayed beaches (Short, 1999). Suggestions that these geological constraints can be as important as dynamic forcing by waves and currents in determining contemporary beach morphology (Jackson et al., 2005) have, however, not been fully realised into the present thinking of beach morphodynamic behaviour (Jackson and Cooper, 2009). Influences of headlands, outcrops, and engineering structures in beach and surfzone dynamics are, nevertheless, frequently acknowledged regarding patterns of wave refraction and attenuation, development of cellular circulation, occurrence of sediment by-passing, and notably in the constraining of cross and longshore processes (e.g. Sanderson and Eliot, 1999; Short, 1999; Larson and Kraus, 2000; Gallop et al., 2011b; Scott et al., 2011).

While the presence of a geological framework is suggested to constrain the ability of a beach to fluctuate both laterally and vertically (Jackson and Cooper, 2009), effects of lateral boundaries, mainly due to headland control on equilibrium shoreline configuration (Silvester, 1985), have traditionally received most of the attention in the embayed beach literature (Ojeda and Guillén, 2008). Under oblique wave conditions, headland protection offers a decreasing lateral sheltering from wave action in the downdrift coastline, promoting the development of a segmented beach based on curvature, energy levels and even textural characteristics (Finkelstein, 1982; Phillips, 1985; Silvester and Hsu, 1997).This lateral boundary effect downdrift of headlands, widely explored in coastal engineering,

decreases as wave obliquity and curvature are reduced, with the entire beach experiencing similar morphological changes (Klein et al., 2010). Irrespective of wave approach angle, as headland spacing decreases and seaward protrusion increases, other lateral boundary effects progressively modify embayed beach response (Short, 1999). In the last decade several studies have investigated the effects of lateral boundaries in natural and artificial embayed beach morphodynamics, focusing on headland restriction and modification of longshore sediment transport that imposes medium- to short-term beach rotation (e.g. Short et al., 2000; Masselink and Pattiaratchi, 2001; Klein et al., 2002, 2010; Ranasinghe et al., 2004; Harley et al., 2008, 2011; Ojeda and Guillén, 2008; Martins et al., 2010; Ruiz de Alegria-Arzaburu and Masselink, 2010; Thomas et al. 2010, 2011; Archetti and Romagnoli, 2011). However, while knowledge of lateral constraints has been advancing, effects of vertical boundaries in the form of submerged non-erodible geological structures (e.g. Larson and Kraus, 2000; Muñoz-Perez and Medina, 2010; Gallop et al., 2011), which also impact the morphological evolution and morphodynamic responses of embayed beaches, have received only limited attention. Few studies have, so far, explored the effects of geological control in beach systems underlain by rocks, often classified as perched beaches (Gallop et al., 2011b). Recently, Jackson and Cooper (2009) presented a conceptual model detailing the general mobility of beaches with varying degrees of underlying geological control. The authors propose three types of beaches based on the relative depth of the vertical boundary (unconstrained, semi-constrained and highly constrained). However, quantitative information about the thickness of sediment veneers below which vertical geological control becomes unimportant remains undetermined (Jackson and Cooper, 2009), and field data describing vertical boundary effects is still scarce (Gallop et al., 2011a).

Various statistical methods have proved to be useful for extracting characteristic behaviour patterns from coastal morphological data (Kroon et al., 2008) and the application of empirical orthogonal functions (EOF) is considered particularly suitable for detecting and quantifying signals from different types of forcing and disturbances (Larson et al., 2003). EOF analysis has been used in beach studies for three decades, following the classical work by Winant et al. (1975), and was recently reviewed by Miller and Dean (2007a; 2007b). Those authors demonstrated the ability of EOF analysis to characterize lateral boundary effects in 20 to 45 km-wide coastal cells, while previous studies using EOF analysis had also highlighted the role of lateral boundaries in embayed beaches (e.g. Clarke and Eliot, 1982; Short et al., 2000). It is therefore naturally appealing to consider EOF analysis as a method for quantitatively characterising the effects of both lateral and vertical boundary effects.

Building on the body of work on the analysis of boundary effects in beach dynamics, this paper explores the range of lateral and vertical geologic constraints on the medium-term (months to years) morphologic behaviour of embayed beaches. Due to similarities between natural headlands and outcrops with engineering structures, an increased knowledge of the mechanisms of geological beach control and boundary effects is important for understanding beach behaviour in the presence of engineering structures that intend to mimic natural geological control in embayed beaches (Hsu et al., 2008). In this paper it is hypothesized that lateral and vertical geological boundaries constrain the morphological behaviour of embayed beaches and that their effects can be decoupled from datasets of embayed beach morphological change. To test this, four specific objectives are outlined:

(i) Decompose the spatial and temporal variability of embayed beach morphology at diverse sites;

(ii) Evaluate the forcing mechanisms driving the observed morphological change;

(iii) Analyse the role of vertical and lateral geological constraints on the morphological response;

(iv) Characterize boundary effects on the morphological behaviour of embayed beaches.

To address the questions and objectives raised, this paper explores EOF analysis, which, although widely used to determine shoreline and beach profile evolution, has been scarcely applied to analyse the evolution of coastal areas controlled by headlands, rocky outcrops or underlying bedrock. Datasets of morphological change from six embayed beaches from southwestern Portugal are used. The beaches are clustered into two groups of three closely located embayments, with beaches within each group exposed to identical offshore forcing. However, due to geological constraints, each beach experiences different morphological changes. The quantitative analysis based on EOF decomposition is complemented by time-variable correlation analysis with several forcing parameters combining hydrodynamic variables, sedimentary and geometric characteristics of each embayment.

2. Field site description

The southwestern coast of Portugal is an indented rocky coastline with marked geodynamic contrasts between the western and southern sections. Despite both being bedrock-framed, with a prevalence of embayed beaches in coastal re-entrants fronting the cliffs or associated with small streams, both geological and environmental characteristics differ significantly between these two sections. Carved in

131 Carboniferous shale and greywacke, the high-energy western coastline is directly exposed to the
132 North Atlantic swell, with several intermediate to dissipative embayed beaches experiencing energetic
133 conditions throughout the year. Mean offshore significant wave heights (H_o) between 1.5 and 2 m, and
134 peak wave periods (T_p) between 9 and 13 s for summer and winter periods, respectively, induce a
135 marked oceanographic seasonality (Costa and Esteves, 2010). Waves reach this coastline
136 predominantly from north-westerly to westerly directions (Fig 1); yet nearly complete refraction of swell
137 waves renders most of these embayed beaches swash aligned. Jurassic to Miocene calcareous cliffs
138 constitute the majority of the rocky section of the southern coastline, which is relatively sheltered from
139 direct exposure to the North Atlantic swell. Offshore wave conditions are moderate, with mean H_o
140 around 0.9 m and mean T_p of 8 s (Costa et al., 2001). Slight variations occur between summer and
141 winter conditions, but not as markedly as on the west coast. Dominant waves reach this coastline from
142 a W-SW direction (Fig. 1), yet shorter period SE waves generated within the Gulf of Cadiz account for
143 roughly a quarter of occurrences (Costa et al., 2001). This oceanographic setting imposes a markedly
144 bimodal wave climate on the sediment-starved, intermediate to reflective south coast embayed
145 beaches. Tidal conditions are identical and nearly synchronous for both sections of the coastline. Tidal
146 regime is classified as semidiurnal and mesotidal, with maximum spring tidal range around 3.5 m.
147 Six embayed beaches were selected as study sites, three in each section of the coastline (Fig. 1).
148 West coast beaches, Amoreira, Mt. Clérigo and Arrifana, are all composed of well-sorted, medium
149 sand, and being exposed to a high-energy wave climate these beaches are modally dissipative or
150 intermediate skewed to dissipative. Amoreira beach is roughly 500 m-long, but is wide and backed by
151 an extensive dune field. This embayment contains a bay-barrier estuary, with a small tidal stream that
152 runs through a shallow channel adjacent to the southern headland. The beach has a persistent low
153 tide terrace, occasionally crossed by the tidal stream, which creates a ridge and runnel-like
154 morphology. Similarly to Amoreira, the Mt. Clérigo embayment faces directly the dominant NW waves.
155 This beach is wide and backed by partly vegetated dunes in the south and central sections, while the
156 northern part is narrow and backed by 50 m-high cliffs. The intertidal area is wide, with rocks
157 outcropping in the southern section of the embayment. Arrifana is a swash-aligned beach, completely
158 enclosed by up to 100 m-high cliffs, and partially protected from dominant NW waves by a prominent
159 northern headland. A lag deposit, composed of coarse gravel and boulders, separates the narrow
160 subaerial beach from the cliffs.
161 The south coast embayments, Salema, Boca do Rio and Cabanas Velhas, are composed of relatively
162 thin layers of medium to coarse sand, which generally overlie lag deposits of cobbles, boulders and/or

shore platforms. These sediment-starved beaches are modally intermediate skewed to reflective. Salema beach is relatively unconstrained by protruding headlands, which allows it to range from 600 to 1100 m in length. Being openly exposed to SSE, this beach receives waves from the dominant SW swell as well as SE sea, which generally impinge on the beach with significant angles. Boca do Rio is a short, narrow beach that corresponds to the terminal part of a small infilled estuary, with a temporary stream that crosses the eastern section of the beach following rainfall events. It is also roughly exposed to SSE, and the reduced seaward protrusion of the bordering headlands also enables waves from both dominant directions to reach the shoreline. Cabanas Velhas is also narrow, and backed by 10 to 50 m-high cliffs. It is exposed directly to the dominant SW waves, being partially protected from SE waves by a protruding eastern headland.

3. Data and methods

3.1 Topographic data

Topographic surveys along cross-shore beach profiles were performed bimonthly on the study sites between September 2007 and September 2009, and complemented by event-driven surveys immediately after storm events and two to three weeks later to monitor beach recovery. Three profiles, with variable alongshore spacing (Fig.1; Table 1), were measured in each embayment using RTK-GNSS (Real Time Kinematic Global Navigation Satellite System). Surveys were undertaken at low tide and extended from the frontal dune or cliff base to the mean low water spring level (MLWS), 1.4 m below mean sea level (MSL), or further seaward.

The selection of proxies to represent the overall beach response is non-trivial. Recent EOF analyses of alongshore beach variability have used datum-based shoreline positions, mainly extracted from time-exposure video images or profile surveys (e.g. Miller and Dean, 2007a; Fairley et al., 2009; Ruiz de Alegría-Arzaburu et al., 2010). These are, however, generally restricted to the upper portion of the cross-shore beach profile. Alternatively, EOF analyses of beach variability have also been performed using a sediment budget approach, using either digital elevation models (e.g. Larson et al., 1999; Haxel and Holman, 2004; Gómez-Pujol et al., 2011), or linear volume along cross-shore beach profiles (e.g. Clarke and Eliot, 1982, 1988). The latter proxy was selected in the present study. Profile volume was computed by trapezoidal integration with the upper limit defined by the profile surface and the MLWS level as lower limit. The MLWS level was chosen because it indicates a vertical morphodynamic separation of the beach profile for exposed beaches in southern Portugal, based on

results presented by Almeida et al. (2011), due to the existence of a nodal point at this level that separates the cross-shore sectors dominated by berm and subtidal terrace changes.

3.2 Empirical orthogonal function analysis

EOF analysis is here applied to decompose the spatial and temporal variability within each dataset. Application of this multivariate statistical technique, often referred as Principal Component Analysis, to coastal geomorphology datasets has been widely described (e.g. Winant et al., 1975; Vincent et al., 1976; Aubrey, 1979; Wijnberg and Terwindt, 1995; Muñoz-Pérez et al., 2001; Dean and Dalrymple, 2002; Larson et al., 2003; Miller and Dean, 2007a). In brief, a data matrix $y(s,t)$ can be represented by a series of linear combinations of spatial and temporal functions, denoted by:

$$y(s,t) = \sum_{k=1}^{n} n_k \, e_k(s) \, c_k(t) \qquad (1)$$

where $e_k(s)$ are the k^{th} spatial eigenfunctions, $c_k(t)$ are the k^{th} temporal eigenfunctions, or temporal coefficients, and n_k the normalizing factor. The new sets of variables, $e_k(s)$ and $c_k(t)$, are orthogonal and therefore, uncorrelated, and ordered in terms of their ability to explain the variance in the original dataset. EOF application allows the dimensionality of a dataset to be reduced (Larson et al., 2003), as generally it is necessary to retain only the first few eigenfunctions, which will account for most of the variance, providing a compact representation of the original data (Miller and Dean, 2007a).

The way the data matrix is specified for EOF analysis is central to the outcome of the calculations (Clarke and Eliot, 1988). The most important distinction involves the scaling of the variables, which were here de-meaned prior to the calculations. Such choice of scale determines that the matrix used to perform the EOF analysis is a covariance matrix. This is the most common option for EOF applications to coastal morphologic data (Larson, et al., 2003), as detailed in recent studies (e.g., Kroon et al., 2008; Fairley et al., 2009; Hansen and Barnard, 2010; Gómez-Pujol et al., 2011). The EOF modes, or eigenfunctions, obtained are thus considered in terms of changes in beach response in regard to the mean ($\Delta V_b^{mean}(t)$ given by $V_b(t_i) - V_b^{mean}$, where V_b is the volume for each survey date t_i and V_b^{mean} is the time averaged volume), which otherwise would tend to dominate the signal (Larson et al., 2003). The first EOF modes are often given physical interpretations based on resemblance of the spatial eigenfunctions with morphological features (e.g. Winant et al., 1975,

Aubrey, 1979), or correlation of temporal eigenfunctions with forcing parameters (e.g. Miller and Dean, 2007b; Fairley et al., 2009).

3.3 Comparison with forcing parameters

Establishing relationships between different variables can provide insights into the behaviour of a beach and how it responds to forcing (Larson et al., 2003). Accordingly, a set of commonly used hydrodynamic and morphodynamic parameters were selected to characterize the forcing and relate it to the temporal eigenfunctions. The variables considered here combine wave, tide, sediment characteristics and embayment geometry, and details of their collection, transformation and application are described below.

3.3.1 Offshore waves and tides

Wave data have been collected by Instituto Hidrográfico (IH) for Portuguese western and southern offshore coastal waters using Datawell directional wave buoys near Sines and Faro (Fig. 1), located both roughly 7 km from shore in approximately 100 m water depths. The buoys provide measurements of offshore significant wave height (H_o), peak spectral period (T_p) and peak wave direction (θ_o). Gaps in the measured wave record, accounting for roughly 15% at Sines and 5% at Faro buoy for the duration of the study, where filled using modelled wave data from WANA deepwater network (Lahoz and Albiach, 2005), provided by Puertos del Estado for grid points near the wave buoys (Fig. 1). Linear correlation analysis indicated a statistically significant correlation between observed and modelled wave heights ($R \geq 0.82$ for $p < 0.01$; RMSE ≤ 0.4m).

Tide level observations and predictions for the west coast beaches were obtained from the IH tide gauge in Sines (Fig. 1). The amount of missing records in the dataset was reduced, around 2%, and these were filled using the predicted tide levels at Sines. Equipment malfunction in Lagos tide gauge (Fig. 1) truncated the observed tide levels, rendering it useless, and predicted tide levels at Lagos were used for the south coast beaches.

3.3.2 Forcing parameters

Numerous dimensional and non-dimensional hydrodynamic and morphodynamic parameters are often used for characterizing the forcing driving beach changes. Ten parameters are considered here, namely breaker height (H_b), breaker angle (θ_b), peak wave period (T_p), wave steepness (H_o/L_o), wave

energy (E_o), wave power (P_o), normalized wave power (Pn_o), alongshore wave energy flux (Pl_b), dimensionless fall velocity (Ω) and the dimensionless embayment scaling parameter (δ').

Deepwater conditions (H_o, T_p and θ_o) are provided directly from the buoy measurements, while breaking conditions (H_b and θ_b) were computed using the formula presented by Larson et al. (2010), developed to derive wave properties at incipient breaking. The use of this simplified solution that employs the conservation of wave energy flux from an offshore location combined with Snell's law for wave refraction disregards wave diffraction around headlands. Although diffraction is an important factor in coastal embayments, this solution was chosen given the reduced headland extend for most study sites and the assumption that the use of such simplified solution is deemed suitable for spatial- and time-averaged shoreline response studies, as it was found adequate to explore the relationships between wave forcing and the temporal eigenfunctions at the scale of interest (meters to kilometres / months to years) (Miller and Dean, 2007b). Depth limited breaking is imposed with the commonly used depth breaker ratio of 0.78. Wave angles were converted in positive/negative angles for waves approaching northwards/southwards to beach normal for the west coast beaches, and waves approaching westwards/eastwards to beach normal for the south coast beaches.

Wave steepness, H_o/L_o, was calculated using linear wave theory with L_o, the deepwater wave length, given by:

$$L_o = (gT_p^2) / (2\pi) \quad (2)$$

where g is the acceleration due to gravity. Offshore wave energy density (E_o), or simply wave energy, was also computed considering linear wave theory:

$$E_o = (1/8)\, pgH_o^2 \quad (3)$$

where ρ is the density of water. Combining wave energy with the deepwater group velocity (C_g) it is possible to compute the rate at which wave energy is transferred by moving waves, the wave power (P_o):

$$P_o = EC_g \quad (4)$$

where C_g is given by

$$C_g = (1 / (4\pi))\, gT_p \quad (5)$$

Recognizing the importance of tidal levels for coastal morphological evolution in Southern Portugal, Morris et al. (2001) proposed the normalized wave power (Pn_o) in order to include the tidal range according to:

$$Pn_o = P_o\,(\eta_{dtr} / \eta_{str}) \quad (6)$$

where η_{dtr} is the maximum daily tidal range and η_{str} is the maximum spring tidal range. This parameter conveniently reflects the enhanced wave erosion potential during spring tides, restricting it for lower tidal ranges (Morris et al., 2001).

In order to obtain an indicator of the alongshore sediment transport, the alongshore component of the wave energy flux (Pl_b) was computed using:

$$Pl_b = (E_b C_g) \sin\theta_b \cos\theta_b \quad (7)$$

where E_b was obtained for breaking conditions according to Eq. (3) replacing H_o by H_b, and C_g as given by the shallow water approximation to wave group velocity:

$$C_g = \sqrt{(g h_b)} \quad (8)$$

where h_b is the water depth at breaking. According to the conversion of wave directions to wave angles positive/negative alongshore energy fluxes correspond to southward/northward transport for west coast beaches, and eastward/westward transport for the south coast beaches.

Besides the purely hydrodynamic parameters presented above, the nearshore forcing can also be represented by parameterizations that incorporate sedimentary characteristics of the embayments. A natural parameter to consider, for its generalized application to beach studies, is the dimensionless fall velocity (Ω) (Gourlay, 1968; Dean, 1973):

$$\Omega = H_b / (W_s T_p) \quad (9)$$

where W_s is the sediment fall velocity, computed according to Soulsby (1997) using the median grain diameter (d_{50}) averaged for each embayment from beach face samples collected seasonally during the two year study period (Table 1).

All the aforementioned parameters are well established in the literature and have proven skilfulness in characterizing morphological changes in the coastal environment. However, no parameter considers explicitly the impact of embayment dimensions and geometry in characterizing the nearshore environment. Short (1996; 1999) based on unpublished work by Marteens and collaborators presented the dimensionless embayment scaling parameter (δ'), which relates the embayment configuration to the incident breaking wave conditions according to:

$$\delta' = S_l^2 / 100 C_l H_b \quad (10)$$

where S_l is the embayment shoreline length and C_l is the chord length (distance between headlands). This empirical approximation was derived from morphometric analysis of embayed beaches in order to describe parametrically the degree of headland impact on surf zone circulation considering a typical surfzone gradient of 0.01 (Short and Masselink, 1999).

3.3.3 Correlation analysis

Linear correlation analysis was used to test the hypothesis that EOF modes have a physical meaning, and are not simply by-products from the mathematical decomposition. Accordingly, if the temporal eigenfunctions of the EOF modes are related to the time series of at least one of the forcing parameters considered, their physical meaning should be elucidated by the characteristics of such forcing parameters (Miller and Dean, 2007b). Correlation between variables was considered statistically significant at the 95% confidence level when the Pearson's product moment correlation coefficient (R) exceeded the critical level ($R_{crit\ 95\%}$) based on two-tailed normal distribution for n-2 degrees of freedom (DOF) (Table 1). More stringent correlation ($R_{crit\ 99\%}$), at the 99% confidence level, is further used in order to distinguish the strongest correlations between the temporal eigenfunctions and the forcing parameters.

As beach changes occur at different frequencies and response times may be site specific, a variable averaging interval for correlation with the temporal eigenfunctions was implemented. The forcing parameters were averaged over 1 to 30 days prior to each survey date, regardless of survey intervals, following Hansen and Barnard (2010) and Alvarez-Ellacuria et al. (2011). As there is no consensus about the optimal averaging interval for correlation of forcing parameters with temporal eigenfunctions (or the beach changes they are supposed to represent), the varying averaging window implemented provides a more flexible approach, enabling further exploration of the response times of each beach. Moreover, by extending from 1 to 30 days (D), the varying averaging window allows the incorporation of daily, weekly and monthly averaging intervals as in other studies (e.g. Miller and Dean, 2007b; Quartel et al., 2008). The averaging interval that produced the first peak in correlation above the critical level was assumed to be the optimal time scale of beach response, regardless of the fact that higher correlation may be obtained for larger averaging windows (refer to Figure 2 for an example of how peak correlation was obtained). The reasoning behind this option is that larger averaging intervals reflect responses to the seasonal variation in wave climate, as suggested by Miller and Dean (2007b), while the first peak in correlation more likely refers to the effects of boundaries in embayed beach response.

4. Results

The results of the EOF decomposition indicate that the first two eigenfunctions explain the majority of morphologic change, accounting for over 95% of the total variability in each embayment (Table 2). The first eigenfunction is undoubtedly the most important, contributing 67% to 94% of the total variance of each dataset, while the second eigenfunction only explains 4% to 29%. The first two eigenfunctions, $e_1(s,t)$ and $e_2(s,t)$, will be analysed in detail bellow, based on the interpretation of spatial patterns and temporal amplitudes for each embayment (Figs. 4-9), and evaluation of their relation with forcing parameters (Table 3).

Over the two-year monitoring period, wave conditions for both sections of the Portuguese southwestern coastline were generally characterized by a concentration of energetic conditions in the periods between November and April, while during the remaining months waves are generally lower, although H_o frequently exceeded 2 m in the west coast and 1 m in the south coast (Fig. 3). Peak wave directions were mostly constant year-round from the NW quadrant in the western section, while for the southern coast there was a striking alternation between SW and SE conditions (Fig. 3). Most

significant events, highlighted in Figure 3, occurred due to rapid succession of high-energy conditions (storm-groups) and waves in excess of 6 m and 4 m for western and southern sections, respectively. Such events were concentrated in the first year of monitoring in the southern coast, while around the western section the most noteworthy event, composed by a group of five storms, occurred later, between late January and mid-February of 2009. This difference in the timing of the most extreme wave conditions had significant implications in the beach behaviour for the two sections of the coastline, as detailed in the following sections.

4.1 Amoreira

The primary mode of variability in Amoreira beach, representing 86% of the variance, consists of a nearly uniform alongshore pattern of beach response. The spatial eigenfunction $e_1(s)$ represents a coherent pattern of morphological change along the entire embayment, although with increased variability in the northern and central sections (Fig. 4). Despite this slight alongshore variation, it is evident that the beach responds as a whole, with changes characterized by alongshore uniform accretion and erosion. From January 2009, the temporal eigenfunction $c_1(t)$ exhibits a marked decrease (Fig.4), most likely related to extreme storm events along the southwestern Portuguese coast reported in Loureiro et al. (2011). Coefficients for $c_1(t)$ remained negative with reduced variation throughout the rest of the monitoring period. The temporal variability of the first eigenfunction is only significantly correlated with the normalized wave power (Pn_o) (Table 3). The negative correlation between $c_1(t)$ and Pn_o, with a peak correlation value of R = -0.51 at D = 1 day, highlights an immediate inverse association between the normalized wave power and beach volume.

The second mode of variability $e_2(s,t)$ accounts for 11% of the variance and exhibits opposing responses for the northern and southern beach ends. This alongshore non-uniform pattern of $e_2(s)$ presents a nodal point located near the centre of the embayment (Fig. 4), and higher variability for the southern section of the beach, adjacent to the stream inlet. Phase shifts between opposing ends of embayed beaches are associated with rotation phenomena (Short, 1999; Klein et al., 2002), and at Amoreira positive/negative phases correspond to clockwise/anticlockwise rotation about the nodal point in the central section of the beach. Mode two temporal eigenfunction $c_2(t)$ is strongly correlated with several forcing parameters (Table 3). Highly significant correlations include the forcing parameters H_b, T_p, E_o, P_o and δ', while Pl_b and Ω are also significantly correlated but at 95% confidence level. The averaging windows for peak correlations with the aforementioned parameters are similar, ranging from 6 to 8 days preceding surveys. Correlation is positive for all these parameters

(except δ'), implying that increases in H_b and T_p, with concomitant increases in E_o, P_o and Ω (and decrease in δ') are translated into a clockwise rotation of the embayment with sediment transferences from the northern section towards the southern section. Anti-clockwise rotation occurs for low waves, and is possibly mediated by the increasing influence of stream discharge and tidal prism under low waves, allowing the development of a secondary stream channel flowing northwards along the foreshore (Freire et al., 2011). Although breaker angle alone lacks any significant correlation with $c_2(t)$, correlation with PI_b provides additional support to the rotation interpretation, as a positive linear relationship implies clockwise (anticlockwise) rotation due to positive-southwards (negative-northwards) alongshore wave energy flux.

4.2 Mt. Clérigo

The spatial eigenfunction$e_1(s)$ at Mt. Clérigo beach indicates a uniform pattern of morphological change, with a slightly higher variability in the central section (Fig. 5). Similarly to Amoreira beach, the combined eigenfunctions for $e_1(s,t)$ (Fig. 5), demonstrate an embayment-wide morphological response, with a seasonal signal. Accretion occurs during summer conditions and erosion in winter. Again, the negative peak after January 2009 marks the occurrence of extreme storm events. This temporal variability of $c_1(t)$ is significantly correlated with Pn_o (R = -0.65 at D = 1). The strong negative correlation peaking at the shorter averaging window suggests a prompt morphological response to changing wave conditions when normalised by the tide.

The second mode eigenfunction for Mt. Clérigo is alongshore non-uniform (Fig. 5). This alongshore non-uniform pattern is consistent with beach rotation behaviour, characterized by the out of phase response between both ends of the embayment (Fig. 5). Significant correlations were found between $c_2(t)$ and the parameters H_b, Ω and δ', with peak values obtained for D = 1 day. While the spatial eigenfunction $e_2(s)$ is consistent with a rotation scenario, the absence of correlation between $c_2(t)$ and the two forcing parameters that include directional information, θ_b and PI_b, indicates that rotation is not likely related with directional forcing. Highly significant correlation with δ' does, however, suggest that surf zone circulation, with development of rip current systems driven by variations in the obliquity of wave approach as proposed by Loureiro et al. (2012), may be the cause of this apparent rotation between opposite extremes of the beach.

4.3 Arrifana

445 Arrifana is the longest yet most indented embayment among the westerly exposed beaches. Mode
446 one eigenfunction $e_1(s,t)$ for this beach follows the general pattern identified for the other embayments.
447 The spatial variability$e_1(s)$ indicates that the beach responds uniformly with both ends experiencing
448 similar, but more extreme, changes than the central section (Fig. 6). The timing of these changes
449 displays identical seasonal signal to the one described for Mt. Clérigo and Amoreira. Several forcing
450 parameters are significantly correlated with $c_1(t)$, (H_b, T_p, E_o, P_o, Pn_o, Pl_b and Ω). Given the particularly
451 strong negative correlation with Pn_o, already noted for the other embayments, but with a wider peak
452 averaging window (D = 12), it is likely that the higher confinement of Arrifana promotes a delayed
453 morphological response comparing to the more exposed embayments, possibly due to enhanced
454 attenuation of the local wave climate.
455 Mode two spatial eigenfunction $e_2(s)$ presents an alongshore non-uniform behaviour, characterized by
456 higher variability in the central section (Fig. 6). Two nodal points occur near the extremities of the
457 beach, lessening the magnitude of changes close to site boundaries for this EOF. None of the forcing
458 parameters is significantly correlated with $c_2(t)$, which restricts the physical interpretation of this mode.
459 Development of circulation cells at the extremities of the beach with onshore re-attachment of sub- to
460 inter-tidal crescentic bars in the central section has been observed in this embayment. These possibly
461 embody a mechanism for beach recovery following rip-induced erosion reported during storms at
462 Arrifana (Loureiro et al., 2012). However, such hypothesis cannot be confirmed, as the forcing
463 parameter *δ'*, which characterizes embayment surfzone circulation, provided no statistically significant
464 support.
465
466 *4.4 Salema*
467 Salema is the embayment where $e_1(s,t)$ ranks the lower relative importance, representing roughly 67%
468 of the variance (Table 2). Absence of nodal points for $e_1(s)$ indicates that morphological changes are
469 synchronous at the entire embayment, with the central and western sectors concentrating the bulk of
470 the variability (Fig. 7). Correlation of $c_1(t)$ is statistically significant with several parameters, as
471 indicated in Table 3, particularly those derived from an energetics-based approach to hydrodynamic
472 forcing. The stronger correlations are again obtained with Pn_o, displaying a negative signal and peak
473 correlations at D = 10 days.
474 Given the lower relative importance of $e_1(s,t)$, mode two eigenfunction $e_2(s,t)$ has a more significant
475 contribution for explaining the variability in Salema dataset (29%). This eigenfunction is consistent with
476 the beach rotation scenario, with a nodal point close to the central section of the beach (Fig. 7). The

combined spatial and temporal eigenfunctions also support the hypothesis of beach rotation, and out-of-phase behaviour is evident in Fig. 7. Correlation analysis of $c_2(t)$ with forcing parameters reinforces this interpretation, with direction-dependent parameters (θ_b and Pl_b) presenting significant correlations, peaking at 6 to 7 days preceding surveys (Table 3). Given the strong association between direction and wave period for the southern Portuguese coast (WSW swell with longer T_p or locally generated SE sea with shorter T_p), both T_p and H_o/L_o present very significant correlations with $c_2(t)$, further emphasising the wave-forced beach rotation scenario.

4.5 Boca do Rio

The primary mode of variability $e_1(s,t)$ in Boca do Rio presents an alongshore uniform pattern of beach change, with slight differences between beach sectors, generally describing a coherent response throughout the entire embayment (Fig. 8). The first mode eigenfunction is marked by a decrease in the temporal amplitude $c_1(t)$ in the first six months of study, followed by an invariant trend, occasionally disturbed by short lived peaks of beach accretion (Fig. 8). This unusual temporal variability is not correlated to any forcing parameter (Table 3) hampering the physical interpretation of mode one in Boca do Rio.

Mode two spatial eigenfunction $e_2(s)$ for Boca do Rio follows the pattern of beach rotation previously described. The strong correlation of $c_2(t)$ with θ_b and Pl_b, for identical averaging windows (Table 3), confirms the hypothesis of a short-term beach rotation scenario at Boca do Rio.

4.6 Cabanas Velhas

Cabanas Velhas primary mode of variability $e_1(s,t)$ is also characterized by a coherent alongshore pattern with higher variability for $e_1(s)$ in the eastern sector (Fig. 9). The chronology of the changes described for Cabanas Velhas $c_1(t)$ is analogous to Boca do Rio $c_1(t)$, but with a sharper decrease in the first few months of study. Strong negative correlations were obtained between $c_1(t)$ and Pn_o, peaking at D = 4 days, reflecting the short-term inverse response to wave conditions along the entire embayment, enhanced by the effects of tidal range variation.

The second mode spatial variability $e_2(s)$ is alongshore non-uniform, with two nodal points closer to the extremes and an area of higher variability in the central section of the embayment (Fig. 9). Variability of $e_2(s,t)$ is consistent with the occurrence of erosion and accretion pulses in the central section of the beach, possibly with a partial contribution to and from the eastern section. Positive correlation values (R = 0.36 to 0.37) and long averaging windows (D = 17 to 18 days) between $c_2(t)$

and wave forcing parameters H_b, E_o, P_o, Ω, suggests that accretionary pulses might occur under moderate to high waves. Although necessarily below the storm threshold value ($H_o \geq 3$ m), higher than average wave forcing is likely to promote the transfer of sediment from the subtidal terrace to the intertidal beach in the bedrock fronted central section of Cabanas Velhas, similar to the effect of large swells in reef-fronted beaches (Miller and Fletcher, 2003).

5. Discussion

5.1 Forcing parameters and response times

Selection of forcing parameters for exploring beach and nearshore morphological behaviour is not obvious or straightforward. Other parameters, reflecting similar nearshore forcing, where considered, for example, by Miller and Dean (2007b) and Fairley et al. (2009) in comparable EOF analysis of morphological change. However, observed significant correlations at the 99% confidence level with at least one of the selected parameters for most eigenfunctions substantiates the validity of our choices. In the results presented here, only two eigenfunctions, $c_2(t)$ in Arrifana and $c_1(t)$ in Boca do Rio, were uncorrelated with the forcing parameters selected. This highlights the case for caution in the interpretation of EOF decompositions, as physical significance of EOF modes can be misleading (Dommenget and Latif, 2002). However, when statistically significant correlation can be identified with meaningful forcing parameters, as shown by the majority of the eigenfunctions analysed, physical interpretation of EOF modes should be considered with confidence (Miller and Dean, 2007b).

From all parameters considered, a marked consistency in strong negative correlation was identified between the first mode eigenfuntion and normalized wave power (Pn_o) in all embayments, with the exception of Boca do Rio. Such correlation agrees with the findings of Fairley et al. (2009), where the first mode eigenfunction of shoreline variability behind detached breakwaters was also negatively correlated with a proxy combining wave and tidal forcing. Pn_o always provides the stronger correlation with $c_1(t)$, highlighting that the incorporation of tidal range variability for normalizing wave power enhances the explanatory ability of this parameter to describe morphological behaviour, as suggested by Morris et al. (2001). This has implications for energetics-based modelling of coastal changes, as this reasoning might be applied to template models of coastal change in meso to macrotidal beaches (e.g. Yates et al., 2009).

Recent modelling and data-analysis work using EOFs on a Mediterranean embayed beach by Alvarez-Ellacuria et al. (2011) indicates a decoupling of response times in morphological behaviour. In

their results, longshore response attributed to the second mode eigenfunction lags cross-shore response associated with the first mode eigenfunction by three days. This decoupling pattern is noticeable in several of the study sites presented here, although not holding consistently for all embayments. Most cases, however, appear to reflect a lag in response times, as evidenced for Amoreira with the first temporal eigenfunction peak correlation at D = 1 day, while the second mode eigenfunction peaks at D = 7 to 8 days (Table 3). Less frequently, both modes peak at the same averaging interval (e.g. Mt. Clérigo with D = 1). Such site-specific response times are likely the result of diverse degrees of exposure and compartmentalization of the various embayments. The general lag for mode two confirms the suggestions of Alvarez-Ellacuria et al. (2011) that the cross-shore and longshore components elucidated do not respond simultaneously, and also of Miller and Dean (2007b) that each mode has a particular response time. Assumptions that on decadal timescales cross-shore processes have a shorter-term response time that longshore processes (Lazarus and Murray, 2007), seem to be applicable also on monthly to seasonal timescales even for highly localized responses. Compartmentalization appears, however, to significantly influence response times, with longer response times in more constrained embayments (e.g. Arrifana).

Given the inclusion of dedicated post-storm surveys in the analysis, a potential bias for faster response times was further investigated considering exclusively the bi-monthly surveys. Results, not shown here, indicate varied behaviour between embayments. Mt. Clérigo and Arrifana presented identical response times considering all surveys and bimonthly surveys only, while Amoreira and Boca to Rio presented slower response times, which increased between 1 and 11 days. In contrast, at Salema response times were 4 to 10 days faster considering only the bimonthly surveys, while at Cabanas Velhas no statistical significant correlations with forcing parameters were found considering exclusively bi-monthly surveys. The reduced number of bimonthly surveys (13) compared to the entire dataset (20 to 33; Table 1) implied higher thresholds for statistical significant correlations ($R_{\text{crit } 95\%} > \pm 0.55$ and $R_{\text{crit } 99\%} > \pm 0.68$), which justify the results observed in Cabanas Velhas, as correlations were already low considering the entire dataset (Table 3). Despite variations in response times, for which no clear storm-related bias was evidenced, most notable changes pertain to the 22% reduction in the forcing parameters for which statistical significant correlations were identified. Again, reduction in survey number and, consequently, more stringent thresholds for statistical significant correlation justifies such variation.

572 *5.2 Mechanisms for alongshore variability*

573 Although early spatial and temporal decompositions of morphological variability using EOF analysis in
574 embayed beaches provide indications that morphological change is associated with nearshore
575 circulation cells (Clarke and Elliot, 1982, 1988; Clarke et al., 1984), most recent studies using this
576 technique have identified beach rotation as the core mechanism of alongshore non-uniformity in
577 embayed beaches (Short et al., 2000; Munõz-Pérez et al., 2001; Short and Trembanis, 2004; Harley
578 et al., 2008; Ruiz de Alegría-Arzaburu et al., 2010). The results shown here, with four beaches
579 presenting second mode eigenfunctions typical of rotation mechanisms, further emphasize the role of
580 beach rotation as a prevailing mode of alongshore variability in embayed beaches. Our results also
581 confirm the ability of EOF analysis to extract the rotation component from diverse datasets. Wave
582 direction-forced beach rotation is, however, not consistently supported for all cases. While at Salema
583 and Boca do Rio statistically significant correlation of $c_2(t)$ with both θ_b and PI_b translates a clear
584 directionally-forced rotation behaviour, expectable under the bi-directional wave climate of southern
585 Portugal, the out of phase pattern observed also in Amoreira and Mt. Clérigo is unlikely to be
586 attributable to a similar mechanism.
587 The appearance of beach rotation (when the extremes of an embayment are out of phase and a nodal
588 point or transition zone exists (Klein et al., 2002)), can in fact be promoted by physical processes other
589 than directionally forced alongshore sediment transport as recently demonstrated by Harley et al.,
590 (2011). Given the strength and signal of the correlation between various forcing and $c_2(t)$ at Amoreira
591 (Table 3), clockwise rotation occurs in this embayment under energetic waves, while anti-clockwise
592 rotation develops during low wave conditions. Such behaviour is most likely the result of complex non-
593 linear interactions involving wave conditions, tidal prisms and fluvial discharge of the shallow coastal
594 stream within Amoreira embayment (Oliveira et al., 2010; Freire et al., 2011). In Mt. Clérigo, the surf
595 zone circulation is suggested as the driver of the out-of-phase response within the embayment for the
596 second mode eigenfunction. Three-dimensional cellular circulation, with extensive rip current systems,
597 has been shown to determine morphological change in Mt. Clérigo (Loureiro et al., 2012). The
598 formation, evolution and clogging of rip and feeder channels, along with the displacement of nearshore
599 bars drives alongshore non-uniform variability producing an inverse response between the extremes
600 of the embayment, similar to findings of Ojeda and Guillén (2008). Strong correlation of $c_2(t)$ with δ' at
601 Mt. Clérigo (Table 3) further validates this hypothesis.
602
603 *5.3 Boundary effects*

Presumed independence of two- and three-dimensional components in coastal morphological change renders EOF decomposition a particularly useful tool for coastal research (Ruessink et al., 2000). Accordingly, nearly all studies of alongshore variability using EOFs in embayed beaches succeeded in isolating the cross-shore component present in the first eigenfunction, describing the bulk of the variability, from the alongshore components in lower-rank eigenfunctions (e.g. Clarke and Eliot, 1982; Short et al., 2000; Harley et al., 2008; Alvarez-Ellacuria et al., 2011). General acceptance of this decoupled morphological response elucidated by the EOF analysis provides a further opportunity to examine the boundary effects in the morphological response of embayed beaches. Vertical boundary effects should be revealed by the variability of the first mode eigenfunction, assumed to represent two-dimensional cross-shore response, while the second mode eigenfunction, embodying three-dimensional alongshore response, ought to portray the effects of lateral boundaries

For all embayments presented here the first mode eigenfunction corresponds to a roughly uniform spatial trend without zero crossings (or nodal points), although not necessarily linear. In the present context, variability in the spatial amplitudes of this eigenfunction is presumed to represent variable two-dimensional geological constraints. Lower $e_1(s)$ amplitudes are indicative of the limitation to free profile fluctuation by underlying hard rock (Clarke and Eliot, 1982; Vousdoukas et al., 2007), implying an effective vertical boundary control on beach profile evolution. The specific mechanisms that determine this constrained dynamics are not yet adequately understood (Gallop et al., 2011b), as they are a result of complex morphodynamic interference of rocky hard-bottoms with beach morphologic change (Larson and Kraus, 2000; Vousdoukas et al., 2007). However, it is generally considered that profile behaviour is dependent on the depth and shape of the underlying geological control (Jackson et al., 2005; Jackson and Cooper, 2009). As such, significant differences exist between the moderate-energy sediment-deprived south coast beaches and the high-energy sediment-richer west coast beaches. Considering both south and west coast embayments in the conceptual framework of Jackson and Cooper (2009), our results place west coast dissipative embayments within the vertical unconstrained beach type, while Salema more likely conforms to the semi-constrained and Boca do Rio and Cabanas Velhas are undoubtedly in the highly-constrained beach type.

South coast embayments, Salema, Boca do Rio and Cabanas Velhas, clearly show evidence of vertical boundary effects, and sectors where underlying geological control is shallower present reduced $e_1(s)$ amplitudes, increasing towards sections with deeper sediment veneers. This gradation can be observed in all three embayments, with the eastern sector in Salema and the western sector in Boca do Rio and Cabanas Velhas displaying minimums in the first mode spatial eigenfuntion (Fig. 7 to

636 Fig. 9). Variable depths of the vertical boundary also imply diverse temporal response for
637 hydrodynamic forced profile modification. Within the south coast beaches, Salema displays temporal
638 variability of $c_1(t)$ broadly consistent with a seasonal forced response, while Boca do Rio and Cabanas
639 Velhas present roughly invariant trends for $c_1(t)$ following severe erosion in the first months of
640 monitoring. Muñoz-Perez et al. (2010) suggested that geologically controlled beach profiles are prone
641 to erosive trends and less able to recover during accretionary periods, and this appears to be the case
642 in the south coast beaches presented here. Thin veneers of sediment covering the underlying rocky
643 substrate in Boca do Rio and Cabanas Velhas were easily eroded in the first months of monitoring.
644 Recovery was limited and both embayments remained depleted by the end of the monitoring period.
645 The limited sediment contained within Salema embayment is, nonetheless, sufficient to enable the
646 development of a sub-aerial beach profile that varies seasonally with significant recovery volumes, as
647 demonstrated by the variability of $c_1(t)$. Such varied behaviour of south coast embayments confirms
648 the suggestions of Muñoz-Perez et al., (2010), further emphasizing an enhancement in recovery ability
649 as sediment depth increases.
650 Vertical boundary effects in west coast beaches are less readily apparent from the first mode
651 eigenfunction. The underlying geological control is significantly deeper and was never exposed for
652 most profiles, yet there are variations in the spatial amplitude of the first mode eigenfunctions,
653 particularly noticeable in Arrifana embayment. Mechanisms other than direct influence of underlying
654 rocky substrate must be considered for the west coast beaches. The highly three-dimensional
655 nearshore behaviour of these high-energy beaches, where large scale rip systems develop during
656 storms and persist for several months (Loureiro et al., 2012), appears to be responsible for the
657 variable spatial amplitudes of $e_1(s)$, as the topographically-controlled location of such rip systems is
658 consistent with the areas of increased variability for $e_1(s)$.
659 Effects of lateral boundaries have received far more attention in studies of morphological variation in
660 embayed beaches, and an established base of literature exists now demonstrating the utility of EOF
661 analysis in extracting the rotation component from morphological change datasets (e.g. Short et al.,
662 2000; Munõz-Pérez et al., 2001; Short and Trembanis, 2004; Miller and Dean, 2007a; Harley et al.,
663 2008; Ruiz de Alegría-Arzaburu et al., 2010). A characteristic rotation pattern for the second mode
664 spatial eigenfunction, with a nodal point separating sectors of inverse morphological response,
665 facilitates interpretation. In most cases, such lateral boundary effects are manifested in embayed
666 beaches through the interruption of longshore sediment transport by a downdrift headland, as a result
667 of seasonal or periodic shifts in wave climate (Short, 1999). When directional forcing can be

associated with the spatial patterns of beach rotation, as in Salema and Boca do Rio, lateral boundaries unequivocally exert their effects by disrupting longshore sediment transport. However, lateral boundary effects can also be manifested through modification of nearshore circulation (Short, 1999). Interpretation of nearshore circulation mechanisms, particularly topographically-controlled rip currents, is not as straightforward as directionally forced beach rotation due to irregular EOF spatial amplitude patterns (Clarke and Eliot, 1982). Nevertheless, correlation with forcing parameters sensitive to beach type and morphodynamic behaviour, notably Ω and δ', does provide indications of the importance of laterally constrained nearshore circulation mechanisms in the three-dimensional behaviour of Cabanas Velhas, Mt. Clérigo and Amoreira embayments.

In coastal embayments it is generally assumed that boundary effects will influence only the sections close to the headlands, leaving a central section relatively unaffected by the site boundaries (Short, 1999; Miller and Dean, 2007a). While this is likely to be the case in wide embayments, the six study sites presented here are clearly small embayments and boundary effects are manifested along the entire beach.

Our original hypothesis that vertical and lateral geological boundaries constrain the morphological behaviour of embayed beaches is abundantly supported by the results. Moreover, although it is not possible to state that the relative importance of two- and three dimensional changes directly relates to the variances explained respectively by the first and second mode eigenfunctions, a clear relation exists between these two variables, as postulated by Ruessink et al. (2000). Such distinction provides support to our secondary hypothesis that boundary effects can be decoupled from datasets of embayed beach morphological change.

Finally, a framework for boundary effects in geologically constrained embayed beaches is proposed (Fig. 10), which considers a basic control on boundary effects by the sedimentary budget. Sediment abundant embayed beaches, with large accommodation spaces, are generally unaffected by vertical boundary effects. They are, however, prone to exhibit lateral boundary effects through constraining of nearshore 3D circulation and/or longshore sediment transport. The relative importance of these processes varies inversely in response to changes in embayment indentation and obliquity of wave approach. Within sediment-deprived embayments the controls on boundary effects are determined mainly by substrate depth and wave obliquity. Increases in both parameters enhance lateral boundary effects, frequently promoting beach rotation, while reductions impose constrains on the cross-shore sediment transport leading to reduced profile fluctuation.

6. Conclusions

This study shows that natural geological boundaries constrain the morphological behaviour of embayed beaches, determining diverse spatial and temporal variability patterns within the six embayments analysed. Localized responses produced by lateral and vertical boundary interference with nearshore dynamics, including beach rotation, topographic-controlled rip circulation and subdued profile fluctuation, are suggested as the primary drivers of alongshore non-uniform morphological variability. Examination of second mode eigenfunction is consistent with recent work suggesting that directionally forced beach rotation is the most frequent mode of alongshore variability in embayed beaches. Rotation patterns can, however, also emerge due to cellular circulation mechanisms or even as a result of complex interactions involving wave conditions, tidal prisms and fluvial discharge of shallow coastal streams.

EOF decomposition confirms suggestions of a spatial decoupling in cross- and longshore responses. Variable peak correlation of temporal amplitudes and forcing parameters also indicates a decoupling in cross- and longshore response times, which appear to increase for more constrained embayments. Highly significant peak correlations of the normalized wave power with the first mode of morphological variability further suggests that, for exposed mesotidal coastal environments, a parameter combining wave and tide variability is likely to increase process-response relations between hydrodynamic forcing and morphological change.

Lateral and vertical geological boundaries exert their effects fundamentally by restraining longshore sediment transport, inducing cellular surf zone circulation and by impacting cross-shore sediment transport. While sediment abundance is suggested as the fundamental element determining boundary effects, embayment indentation, wave obliquity and substrate depth are considered decisive to determine the morphological impact of vertical and lateral geological boundaries.

Acknowledgements

This work is a contribution to Project BAYBEACH – Evolution and Management of Embayed Beaches in Contrasting Environments, funded by FCT under contract PTDC/CTE-GEX/66893/2006. Carlos Loureiro was supported by FCT, grant reference SFRH/BD/27878/2006. Hydrodynamic data was provided by Instituto Hidrográfico. Modelled WANA wave data were supplied by Puertos del Estado. We gratefully acknowledge the help of everyone involved in the fieldwork data collection, frequently

under severe weather conditions. We are especially grateful to Mara Nunes (CIMA - UALG) for valuable assistance during surveying and Lluís Gómez-Pujol (SOCIB - IMEDEA) for thoughtful insights and documentation regarding EOF analysis.

References

Almeida, L.P., Ferreira, Ó., Pacheco, A., 2011. Thresholds for morphological changes on an exposed sandy beach as a function of wave height. Earth Surface Processes and Landforms 36, 523-532.

Archetti, R., Romagnoli, C., 2011. Analysis of the effects of different storm events on shoreline dynamics of an artificially embayed beach. Earth Surface Processes and Landforms 36, 1449-1463.

Aubrey, D.G., 1979. Seasonal patterns of onshore/offshore sediment movement. Journal of Geophysical Research 84 (C10), 6347-6354.

Clarke, D.J., Eliot, I.G., 1982. Description of littoral, alongshore sediment movement from empirical eigen-function analysis. Journal of the Geological Society of Australia 29, 327-341.

Clarke, D.J., Eliot, I.G., 1988. Low-frequency changes of sediment volume on the beachface at Warilla beach, New South Wales, 1975-1985. Marine Geology 79, 189-211.

Clarke, D.J., Eliot, I.G., Frew, J.R., 1984. Variation in subaerial beach sediment volume on a small sandy beach over a monthly lunar tidal cycle. Marine Geology 58, 319-344.

Costa, M., Esteves, R., 2010. Clima de agitação marítima na costa oeste de Portugal Continental. Proceedings of XI Jornadas Técnicas de Engenharia Naval – O Sector Marítimo Português. Edições Salamadra, Lisboa. 413-426.

Costa, M., Silva, R., Vitorino, J., 2001. Contribuição para o estudo do clima de agitação marítima na costa Portuguesa. Proceedings of 2as Jornadas de Engenharia Costeira e Portuária. AIPCN, Aveiro, 20 p. (CD-ROM).

Dean, R.G., 1973. Heuristic models of sand transport in the surf zone. Proceedings of the Conference on Engineering Dynamics in the Surfzone. Institute of Engineers, Sydney, Australia, 208-214.

Dean, R.G., Dalrymple, R.A., 2002. Coastal Processes with Engineering Applications. Cambridge University Press, Cambridge.

Dommenget, D., Latif, M., 2002. A cautionary note on the interpretation of EOFs. Journal of Climate 15, 216-225.

Fairley, I., Davidson, M., Kingston, K., Dolphin, T., Philips, R., 2009. Empirical orthogonal function analysis of shoreline changes behind two different designs of detached breakwaters. Coastal Engineering 56, 1097-1108.

Finkelstein, K., 1982. Morphological variations and sediment transport in crenulate-bay beaches, Kodiak Island, Alaska. Marine Geology 47, 261-281.

768 Freire, P., Taborda, R., Bertin, X., Guerreiro, M., Fortunato, A.B., Silva, A.M., Andrade, C., Oliveira, A.,
769 Antunes, C., Freitas, M.C., Nahon, A., Rodrigues, M., Bruneau, N., 2011. Medium-term
770 morphodynamic evolution of a small coastal inlet. Journal of Coastal Research SI 64, 666-670.

771 Gallop, S.L., Bosserelle, C., Pattiaratchi, C.B., Eliot, I., 2011a. Hydrodynamic and morphological
772 response of a perched beach during sea breeze activity. Journal of Coastal Research SI 64, 78-
773 79.

774 Gallop, S.L., Bosserelle, C., Pattiaratchi, C.B., Eliot, I., 2011b. Rock topography causes spatial
775 variation in the wave, current and beach response to sea breeze activity. Marine Geology 290, 29-
776 40.

777 Gómez-Pujol, L., Orfila, A., Álvarez-Ellacuría, A., Tintoré, J., 2011. Controls on sediment dynamics
778 and medium-term morphological change in a barred microtidal beach (Cala Millor, Mallorca,
779 Western Mediterranean). Geomorphology 132, 87-98.

780 Gourlay, M.R., 1968. Beach and Dune Erosion Tests I. Report M935/M936, Delft Hydraulics
781 Laboratory, 117 p.

782 Hansen, J.E., Barnard, P.L. 2010. Sub-weekly to interannual variability of a high-energy shoreline.
783 Coastal Engineering 57, 959-972.

784 Harley, M.D., Turner, I.L., Short, A.D, Ranasinghe, R., 2008. Rotation and oscillation of an embayed
785 beach. Proceedings of the 31st International Conference on Coastal Engineering. World Scientific
786 Publishing, Singapore. 865-875.

787 Harley, M.D., Turner, I.L., Short, A.D, Ranasinghe, R., 2011. A reevaluation of coastal embayment
788 rotation: the dominance of cross-shore versus alongshore transport processes, Collaroy-
789 Narrabeen Beach, southeast Australia. Journal of Geophysical Research 116, F040033.

790 Haxel, J.H., Holman, R.A., 2004. The sediment response of a dissipative beach to variations in wave
791 climate. Marine Geology 206 73-99.

792 Hsu, J.R.C., Benedet, L., Klein, A.H.F., Raabe, A.L.A., Tsai, C.P., Hsu, T.W., 2008. Appreciation of
793 static bay beach concept for coastal management and protection. Journal of Coastal Research
794 24, 198-215.

795 Jackson, D.W.T., Cooper, J.A.G., 2009. Geological control on beach form: accommodation space and
796 contemporary dynamics. Journal of Coastal Research SI 56, 69-72.

797 Jackson, D.W.T., Cooper, J.A.G., del Rio, L., 2005. Geological control of beach morphodynamic state.
798 Marine Geology 216, 297-314.

799 Klein, A.H.F, Benedet, L., Schumacher, D.H., 2002. Short-term beach rotation processes in distinct
800 headland bay beach systems. Journal of Coastal Research 18, 442-458.

801 Klein, A.H.F, Ferreira, Ó., Dias, J.M.A., Tessler, M.G., Silveira, L.F., Benedet, L., Menezes, J.T.,
802 Abreu, J.G.N., 2010. Morphodynamics of structurally controlled headland-bay beaches in
803 southeastern Brazil: a review. Coastal Engineering 57, 98-111.

804 Kroon, A., Larson, M., Möller, I., Yokoki, H., Rozynsky, G., Cox, J., Larroude, P., 2008. Statistical
805 analysis of coastal morphological data sets over seasonal to decadal time scales. Coastal
806 Engineering 55, 581-600.

807 Lahoz, M.G., Albiach, J.C.C., 2005. Wave forecasting at the Spanish coasts. Journal of Atmospheric &
808 Ocean Science 10, 389-405.

809 Larson, M., Capobianco, M., Jansen, H., Rózynski, G., Southgate, H.N., Stive, M., Wijnberg, K.M.,
810 Hulscher, S., 2003. Analysis and modelling of field data on coastal morphological evolution over
811 yearly and decadal time scales. Part 1: background and linear techniques. Journal of Coastal
812 Research 19, 760-775.

813 Larson, M., Hanson, H., Kraus, N.C., Newe, J., 1999. Short- and long-term responses of beach fills
814 determined by EOF analysis. Journal of Waterway, Port, Coastal and Ocean Engineering 125,
815 285-293.

816 Larson, M., Hoan, L.X., Hanson, H., 2010. Direct formula to compute wave height and angle at
817 incipient breaking. Journal of Waterway, Port, Coastal and Ocean Engineering 136, 119-122.

818 Larson, M., Kraus, N.C., 2000. Representation of non-erodible (hard) bottoms in beach profile change
819 modelling. Journal of Coastal Research 16, 1-14.

820 Lazarus, E.D., Murray, A.B., 2007. Process signatures in regional patterns of shoreline change on
821 annual to decadal time-scales. Geophysical Research Letters 34, L19402.

822 Loureiro, C., Ferreira, Ó., Cooper, J.A.G., 2011. Morphologic change and morphodynamics at high-
823 energy embayed beaches in southwestern Portugal. Proceedings of Coastal Sediments '11.
824 World Scientific Publishing, Singapore. Vol. 2, 1375-1389.

825 Loureiro, C., Ferreira, Ó., Cooper, J.A.G., 2012. Extreme erosion on high-energy embayed beaches:
826 influence of megarips and storm groups. Geomorphology (in press).
827 DOI:10.1016/j.geomorph.2011.10.013.

828 Martins, C.C., Mahiques, M.M., Dias, J.M.A., 2010. Daily morphological changes determined by high-
829 energy events on an embayed beach: a qualitative model. Earth Surface Processes and
830 Landforms 35, 487-495.

831 Masselink, G., Pattiaratchi, C.B., 2001. Seasonal changes in beach morphology along the sheltered
832 coastline of Perth, Western Australia. Marine Geology 172, 243-263.

833 Miller, J.K., Dean, R.G., 2007a. Shoreline variability via empirical orthogonal function analysis: Part I
834 temporal and spatial characteristics. Coastal Engineering 54, 111-131.

835 Miller, J.K., Dean, R.G., 2007b. Shoreline variability via empirical orthogonal function analysis: Part II
836 relationship to nearshore conditions. Coastal Engineering 54, 133-150.

837 Miller, T.L., Fletcher, C.H., 2003. Waikiki: historical analysis of an engineered shoreline. Journal of
838 Coastal Research 19, 1026-1043.

839 Morris, B.D., Davidson, M., Huntley, D., 2001. Measurements of the response of a coastal inlet using
840 video monitoring techniques. Marine Geology 175, 251-272.

841 Muñoz-Perez, J.J., Medina, R., 2010. Comparison of long-, medium- and short-term variations of
842 beach profiles with and without submerged geological control. Coastal Engineering 57, 241-251.

843 Muñoz-Pérez, J.J., Medina, R., Tejedor, B., 2001. Evolution of longshore beach contour lines
844 determined by the E.O.F. method. Scientia Marina 65, 393-402.

845 Ojeda, E., Guillén, J., 2008. Shoreline dynamics and beach rotation of artificial embayed beaches.
846 Marine Geology 253, 51-62.

847 Oliveira, A., Fortunato, A.B., Guerreiro, M., Bertin, X., Bruneau, N., Rodrigues, M., Taborda, R.,
848 Andrade, C., Silva, A.M., Antunes, C., Freire, P., Pedro, S.L., Dodet, G., Loureiro, C., Mendes, A.,
849 2010. Effect of inlet morphology and wave action on transport and sediment dynamics in a coastal
850 stream. Proceedings of the Eleventh International Conference on Estuarine and Coastal
851 Modeling. ASCE Conference Proceedings 388, 601-620.

852 Phillips, J.D., 1985. Headland-bay beaches revisited: an example from Sandy Hook, New Jersey.
853 Marine Geology 65, 21-31.

854 Quartel, S., Kroon, A., Ruessink, B.G., 2008. Seasonal accretion and erosion patterns of a microtidal
855 sandy beach. Marine Geology 250, 19-33.

856 Ranasinghe, R., McLoughlin, R., Short, A.D., Symonds, G., 2004. The Southern Oscillation Index,
857 wave climate and beach rotation. Marine Geology 204, 273-287.

858 Ruessink, B.G., van Enckevort, I.M.J., Kingston, K.S., Davidson, M.A., 2000. Analysis of observed
859 two- and three-dimensional nearshore bar behaviour. Marine Geology 169, 161-183.

860 Ruiz de Alegría-Arzaburu, A., Masselink, G., 2010. Storm response and beach rotation on a gravel
861 beach, Slapton Sands, UK. Marine Geology 278, 77-99.

862 Ruiz de Alegría-Arzaburu, A.R., Pedrozo-Acuña, A., Horrillo-Caraballo, J.M., Masselink, G., Reeve,
863 D.E., 2010. Determination of wave-shoreline dynamics on a macrotidal gravel beach using
864 Canonical Correlation Analysis. Coastal Engineering 57, 290-303.

865 Sanderson, P.G., Eliot, I., 1999. Compartmentalisation of beachface sediments along the
866 southwestern coast of Australia. Marine Geology 162, 145-164.

867 Scott, T., Masselink, G., Russel, P., 2011. Morphodynamic characteristics and classification of
868 beaches in England and Wales. Marine Geology 286, 1-20.

869 Short, A.D., 1996. The role of wave height, period, slope, tide range and embaymentisation in beach
870 classifications: a review. Revista Chilena de Historia Natural 69, 589-604.

871 Short, A.D., 1999. Handbook of Beach and Shoreface Morphodynamics. John Wiley & Sons,
872 Chichester.

873 Short, A.D., 2010. Role of geological inheritance in Australian beach morphodynamics. Coastal
874 Engineering 57, 92-97.

875 Short, A.D., Trembanis, A.C., Turner, I.L., 2000. Beach oscillations, rotation and the southern
876 oscillation , Narrabeen Beach, Australia. Proceedings of the 27th International Conference on
877 Coastal Engineering. ASCE, Sydney. 2439-2452.

878 Short, A.D., Trembanis, A.C., 2004. Decadal scale patterns in beach oscillation and rotation,
879 Narrabeen Beach, Australia – time series, PCA and wavelet analysis. Journal of Coastal
880 Research 20, 523-532.

881 Silvester, R., 1985. Natural headland control of beaches. Continental Shelf Research, 4, 581-596.

882 Silvester, R., Hsu, J.R.C., 1997. Coastal Stabilization. World Scientific, Singapore. 578 p.

883 Soulsby, R.L., 1997. Dynamics of Marine Sands: a manual for practical applications. Thomas Telford,
884 London.

885 Thomas, T., Phillips, M.R., Williams, A.T., 2010. Mesoscale evolution of a headland bay: beach
886 rotation processes. Geomorphology 123, 129-141.

887 Thomas, T., Phillips, M.R., Williams, A.T., Jenkins, R.E., 2011. Short-term beach rotation, wave
888 climate and the North Atlantic Oscillation (NAO). Progress in Physical Geography 35, 333-352.

889 van Enckevort, I.M.J., Ruessink, B.G., 2003. Video observations of nearshore bar behaviour. Part 2:
890 alongshore non-uniform variability. Continental Shelf Research 23, 513-532.

891 Vincent, L., Dolan, R., Hayden, Resio, D., 1976. Systematic variations in barrier-island topography.
892 Journal of Geology 84, 583-594.

893 Vousdoukas, M.I., Velegrakis, A.F., Plomaritis, T.A., 2007. Beachrock occurrence, characteristics,
894 formation mechanisms and impacts. Earth-Science Reviews 85, 23-46.

895 Vousdoukas, M.I., Velegrakis, A.F., Karambas, T.V., 2009. Morphology and sedimentology of a
896 microtidal beach with beachrocks: Vatera, Lesbos, NE Mediterranean. Continental Shelf
897 Research 29, 1937-1947.

898 Wijnberg, K.M., Terwindt, J.H.J., 1995. Extracting decadal morphological behaviour from high-
899 resolution, long-term bathymetric surveys along the Holland coast using eigenfunctions analysis.
900 Marine Geology 126, 301-330.

901 Winant, C.D., Inman, D.L., Nordstrom, C.E., 1975. Description of seasonal beach changes using
902 empirical eigenfunctions. Journal of Geophysical Research 80, 1979-1986.

903 Yates, M.L., Guza, R.T., O'Reilly, W.C., 2009. Equilibrium shoreline response: observations and
904 modelling. Journal of Geophysical Research 114, C09014.

905

906

907

908

909

910

911

912

List of Tables

List of Figures

974 spatial and temporal eigenfunctions (lower panels). North, Centre and South are relative to the profiles
975 location at the beach.
976
977 **Figure 7** – Normalized spatial ($e_n(s)$) and temporal ($c_n(t)$) eigenfunctions for Salema beach dataset
978 (upper panels). Reconstruction of the first two EOF modes, based on the combined analysis of the
979 spatial and temporal eigenfunctions (lower panels). West, Centre and East are relative to the profiles
980 location at the beach.
981
982 **Figure 8** – Normalized spatial ($e_n(s)$) and temporal ($c_n(t)$) eigenfunctions for Boca do Rio beach
983 dataset (upper panels). Reconstruction of the first two EOF modes, based on the combined analysis of
984 the spatial and temporal eigenfunctions (lower panels). West, Centre and East are relative to the
985 profiles location at the beach.
986
987 **Figure 9** – Normalized spatial ($e_n(s)$) and temporal ($c_n(t)$) eigenfunctions for Cabanas Velhas beach
988 dataset (upper panels). Reconstruction of the first two EOF modes, based on the combined analysis of
989 the spatial and temporal eigenfunctions (lower panels). West, Centre and East are relative to the
990 profiles location at the beach.
991
992 **Figure 10** – Conceptual framework describing boundary effects in embayed beaches
993
994

Figure 1
Click here to download high resolution image

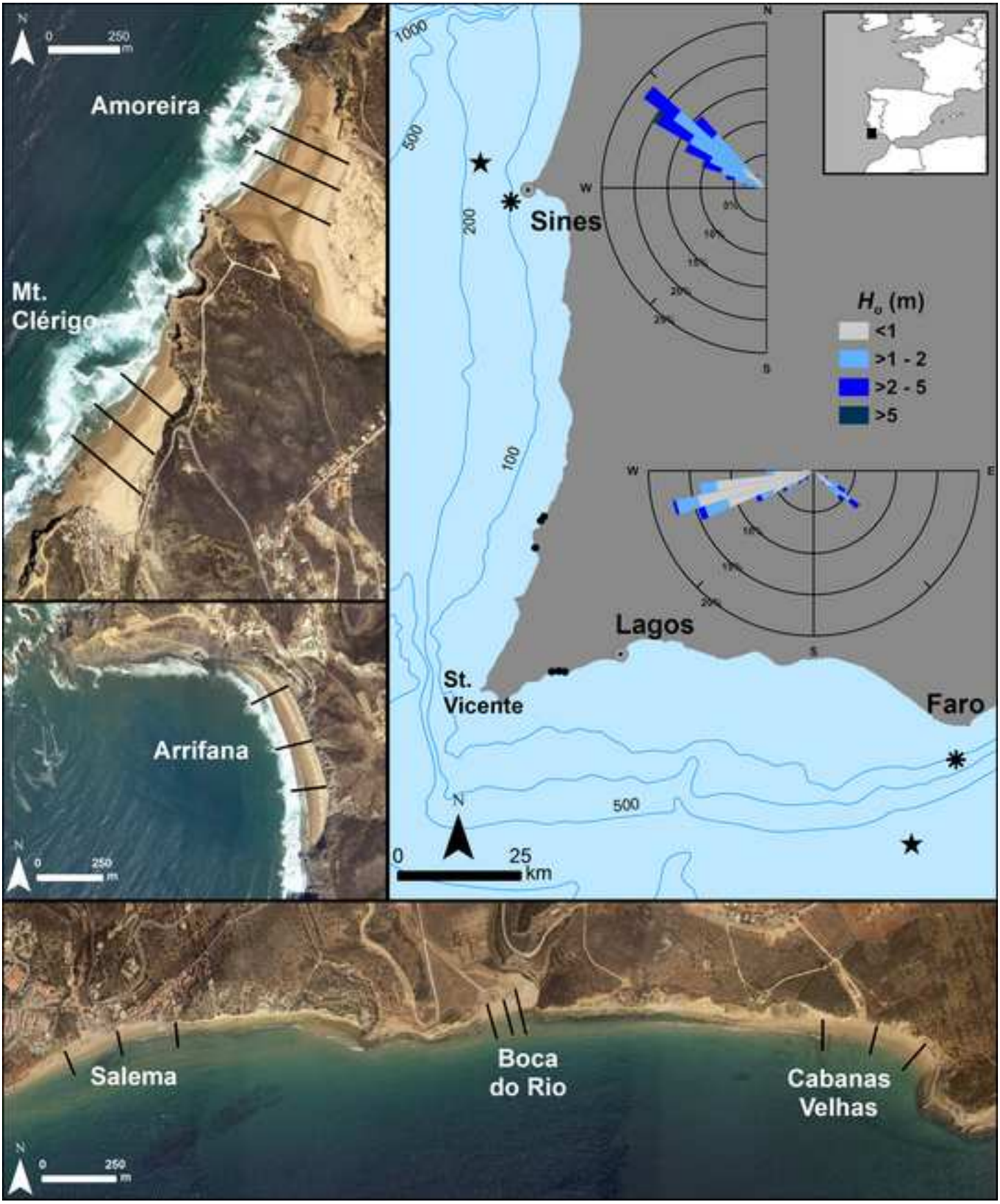

Figure 2

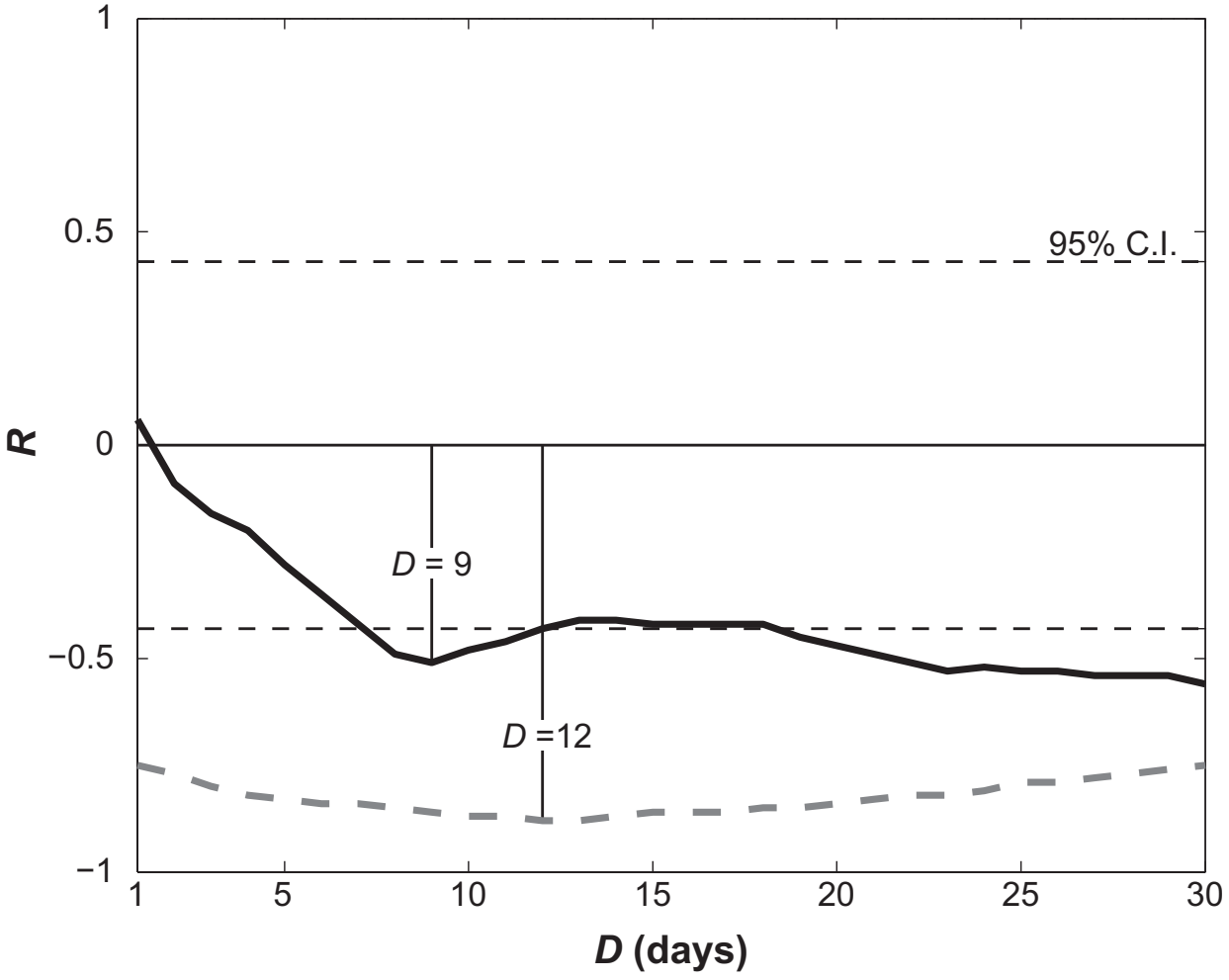

Figure 3

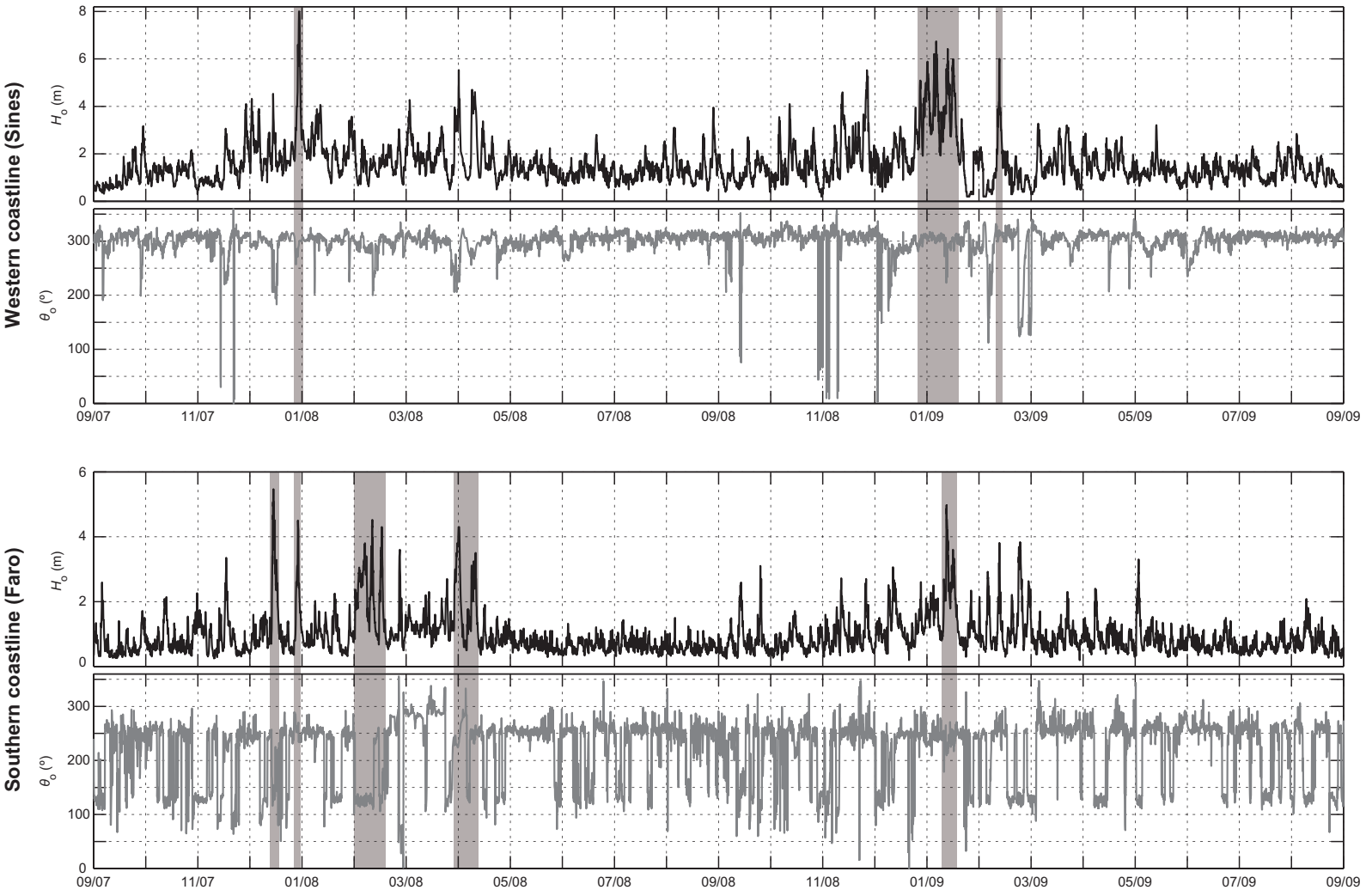
Western coastline (Sines)
H_o (m)
θ_o (°)
0
2
4
6
8
100
200
300
09/07
11/07
01/08
03/08
05/08
07/08
09/08
11/08
01/09
03/09
05/09
07/09
09/09

Southern coastline (Faro)
H_o (m)
θ_o (°)
0
2
4
6
100
200
300
09/07
11/07
01/08
03/08
05/08
07/08
09/08
11/08
01/09
03/09
05/09
07/09
09/09

Figure 4

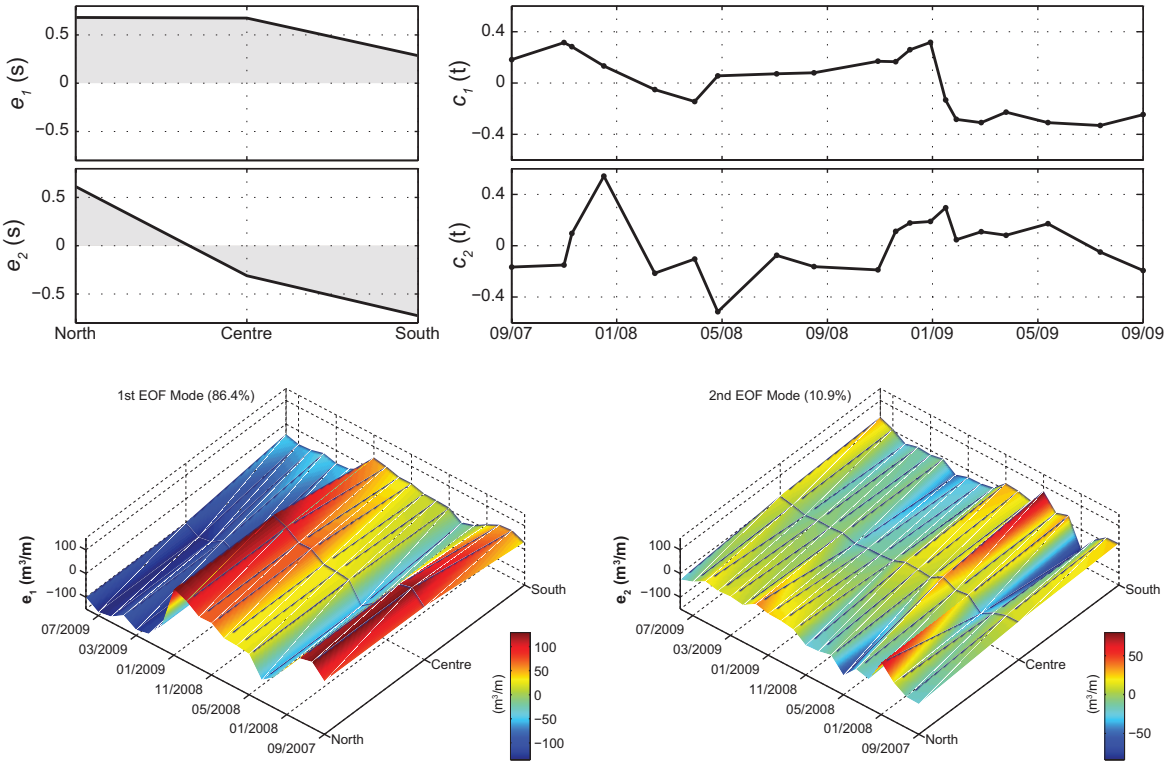
0.5
0
−0.5
e_1 (s)
e_2 (s)
North
Centre
South
0.4
0
−0.4
c_1 (t)
c_2 (t)
09/07
01/08
05/08
09/08
01/09
05/09
09/09
1st EOF Mode (86.4%)
2nd EOF Mode (10.9%)
e_1 (m³/m)
e_2 (m³/m)
100
0
−100
07/2009
03/2009
01/2009
11/2008
05/2008
01/2008
09/2007
South
Centre
North
(m³/m)
50
−50

Figure 5

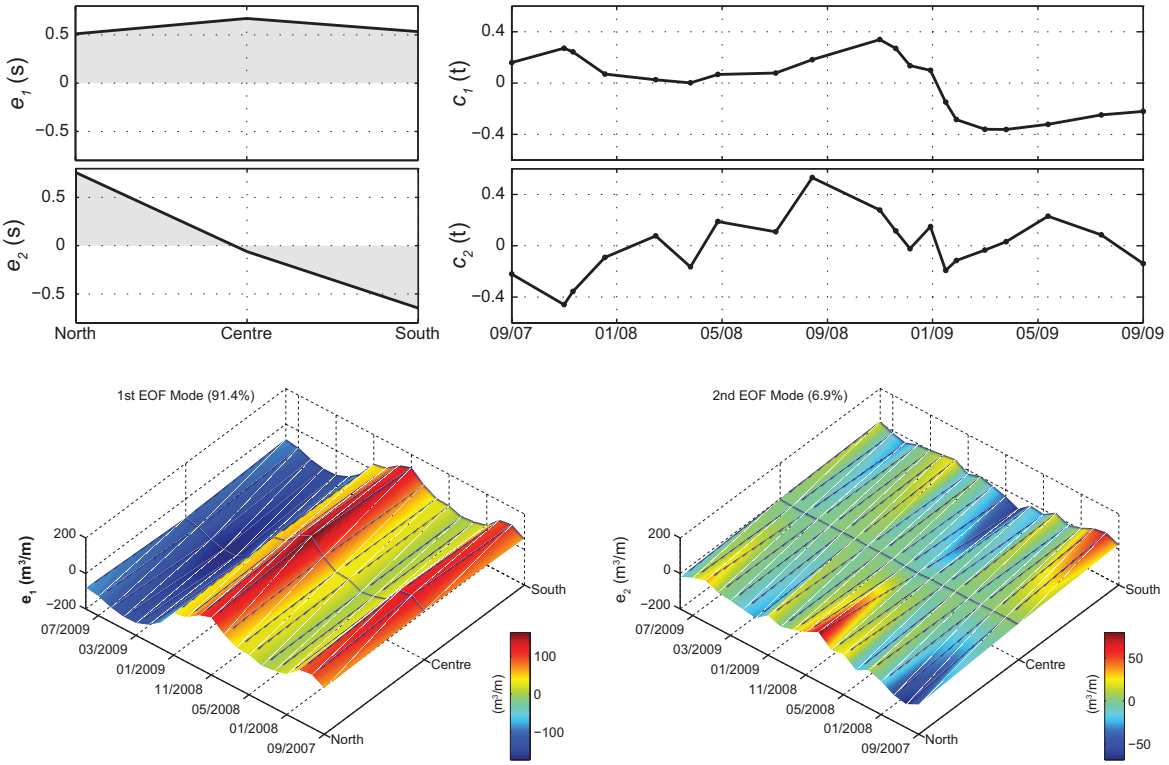
0.5
0
−0.5
e1 (s)
e2 (s)
North
Centre
South
0.4
−0.4
c1 (t)
c2 (t)
09/07
01/08
05/08
09/08
01/09
05/09
09/09
1st EOF Mode (91.4%)
2nd EOF Mode (6.9%)
e1 (m3/m)
e2 (m3/m)
200
0
−200
07/2009
03/2009
01/2009
11/2008
05/2008
01/2008
09/2007
South
Centre
North
100
0
−100
50
−50
(m3/m)

Figure 6

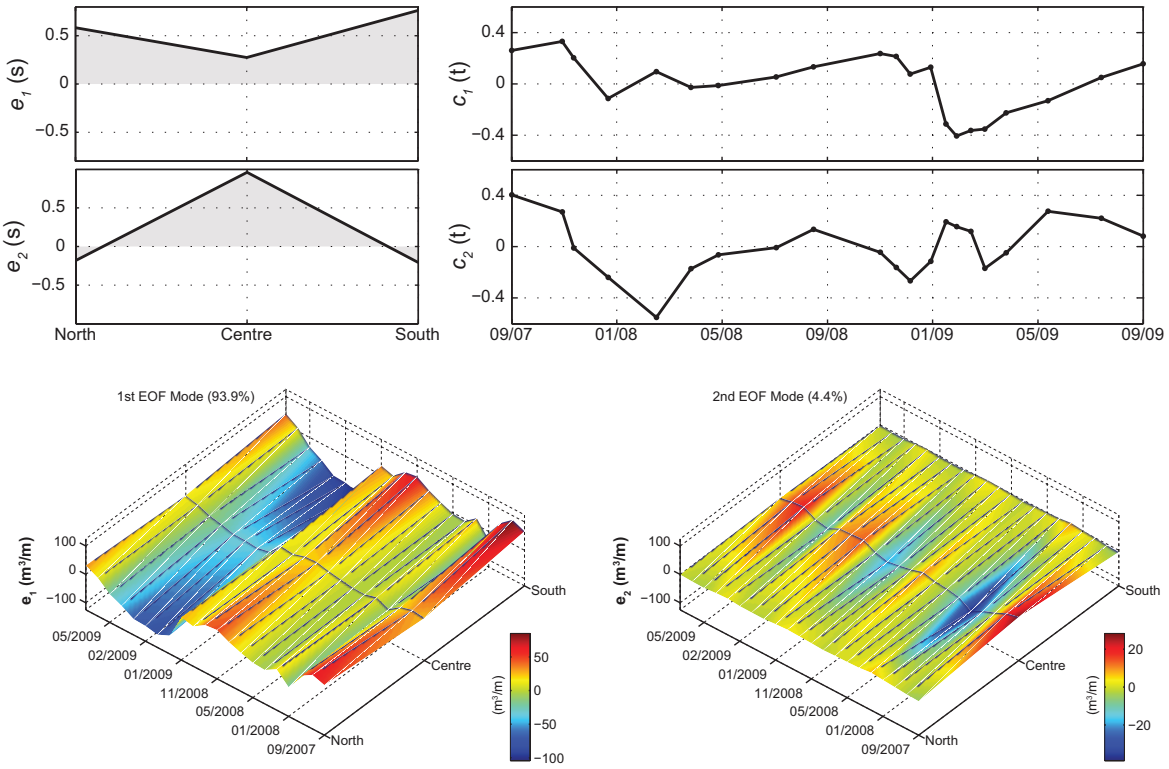
0.5
0
−0.5
e1 (s)
e2 (s)
North
Centre
South
0.4
0
−0.4
c1 (t)
c2 (t)
09/07
01/08
05/08
09/08
01/09
05/09
09/09
1st EOF Mode (93.9%)
2nd EOF Mode (4.4%)
e1 (m³/m)
e2 (m³/m)
100
0
−100
05/2009
02/2009
01/2009
11/2008
05/2008
01/2008
09/2007
South
Centre
North
50
0
−50
−100
20
0
−20
(m³/m)

Figure 7

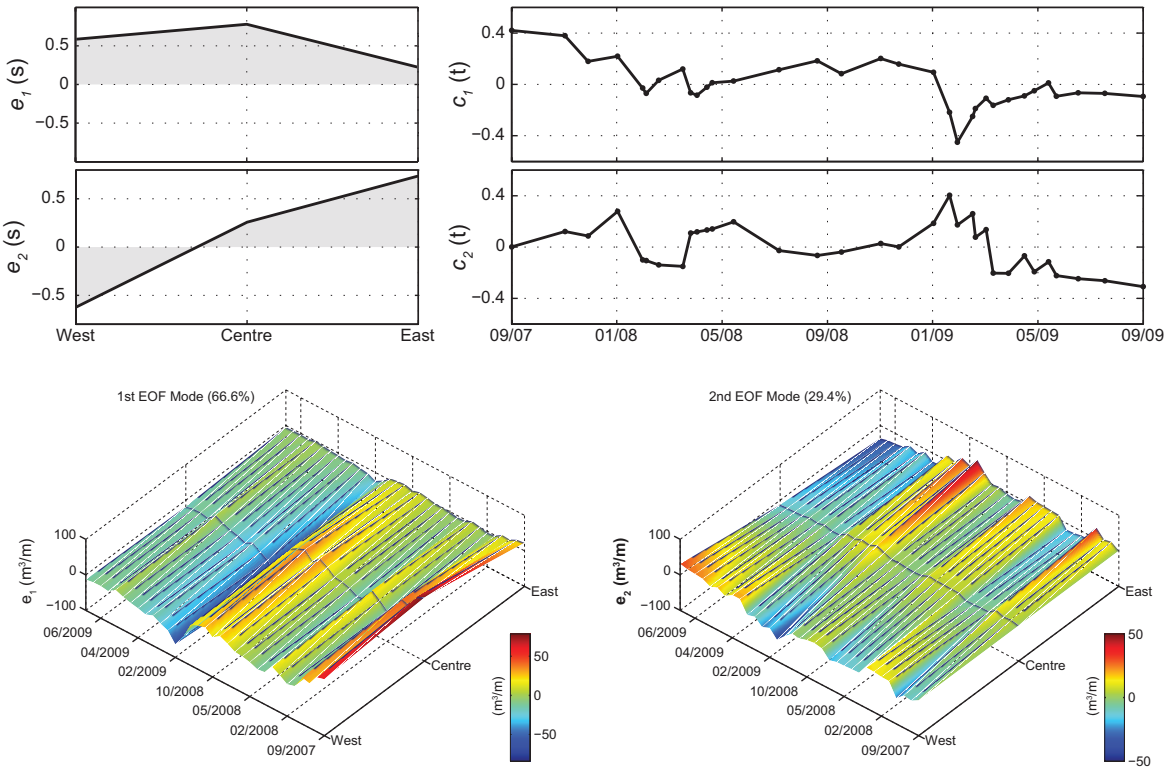
0.5
0
−0.5
e1 (s)
e2 (s)
West
Centre
East
0.4
−0.4
c1 (t)
c2 (t)
09/07
01/08
05/08
09/08
01/09
05/09
09/09
1st EOF Mode (66.6%)
2nd EOF Mode (29.4%)
e1 (m3/m)
e2 (m3/m)
100
−100
06/2009
04/2009
02/2009
10/2008
05/2008
02/2008
09/2007
East
Centre
West
50
−50
(m3/m)

Figure 8

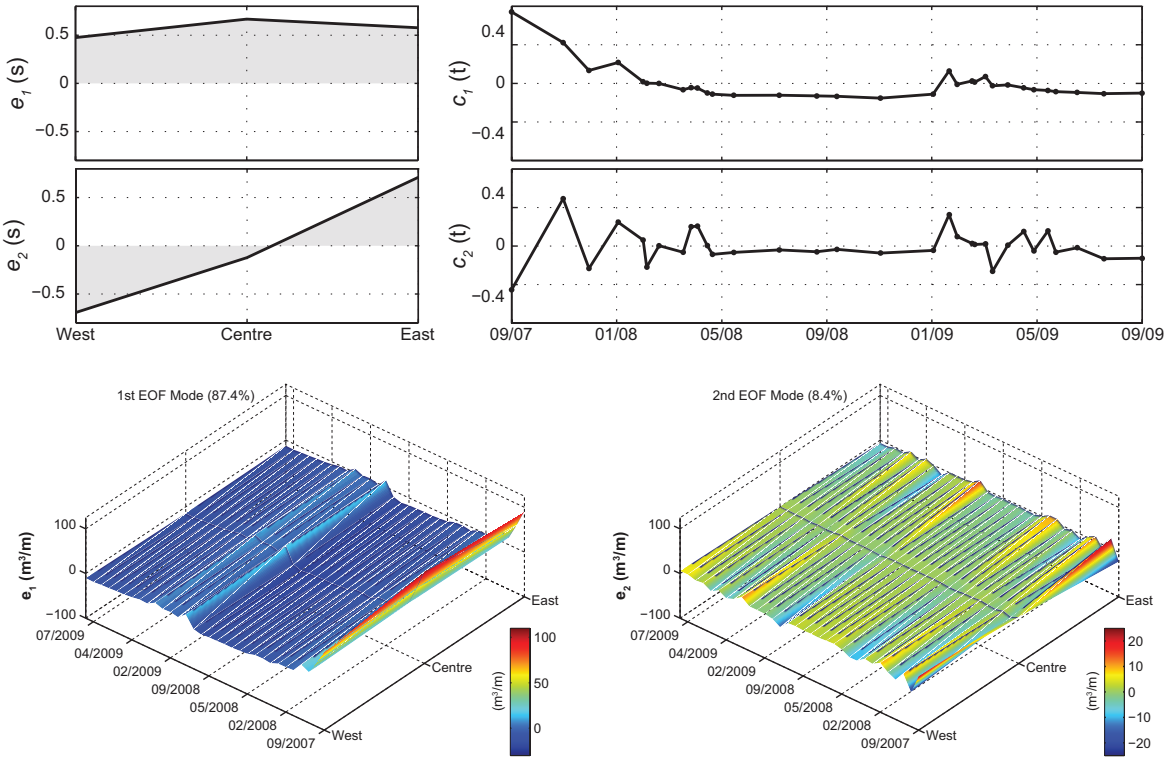
0.5
0
−0.5
e_1 (s)
e_2 (s)
West
Centre
East
0.4
−0.4
c_1 (t)
c_2 (t)
09/07
01/08
05/08
09/08
01/09
05/09
09/09
1st EOF Mode (87.4%)
2nd EOF Mode (8.4%)
e_1 (m³/m)
e_2 (m³/m)
100
−100
07/2009
04/2009
02/2009
09/2008
05/2008
02/2008
09/2007
East
Centre
West
(m³/m)
50
20
10
−10
−20

Figure 9

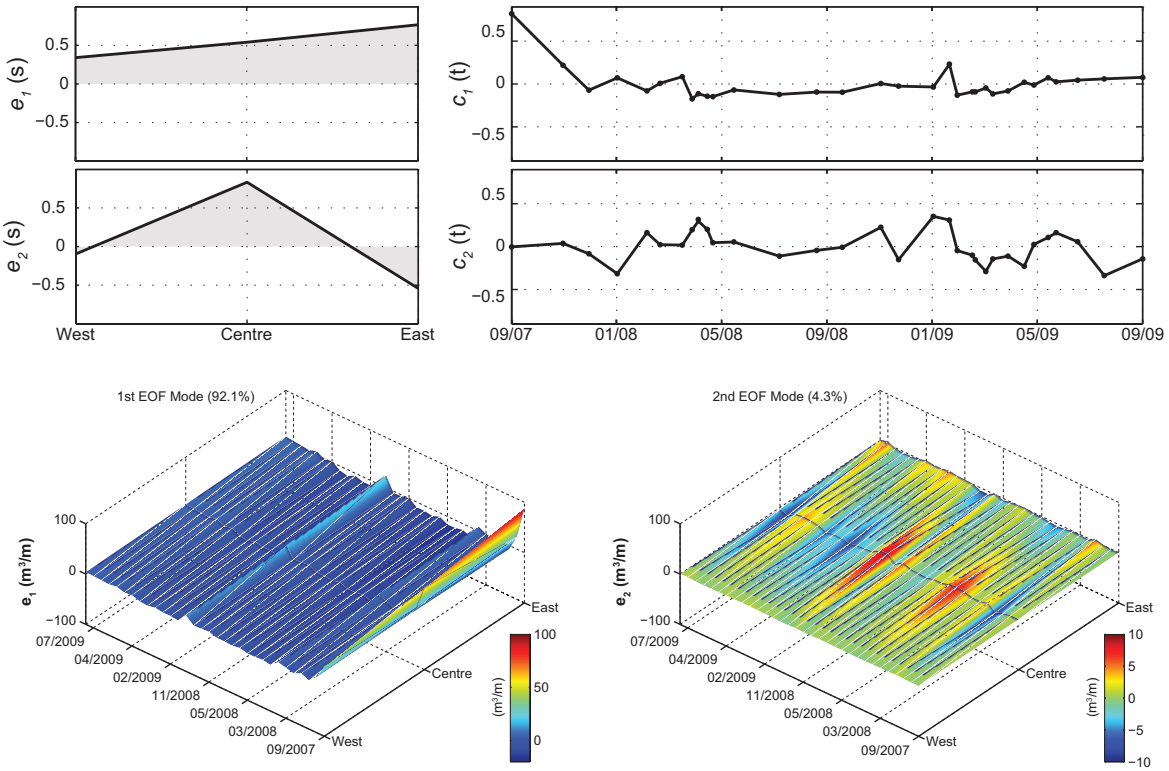
0.5
0
−0.5
e_1 (s)
e_2 (s)
West
Centre
East
c_1 (t)
c_2 (t)
09/07
01/08
05/08
09/08
01/09
05/09
09/09
1st EOF Mode (92.1%)
2nd EOF Mode (4.3%)
e_1 (m³/m)
e_2 (m³/m)
100
0
−100
07/2009
04/2009
02/2009
11/2008
05/2008
03/2008
09/2007
East
Centre
West
(m³/m)
50
10
5
−5
−10

Figure 10

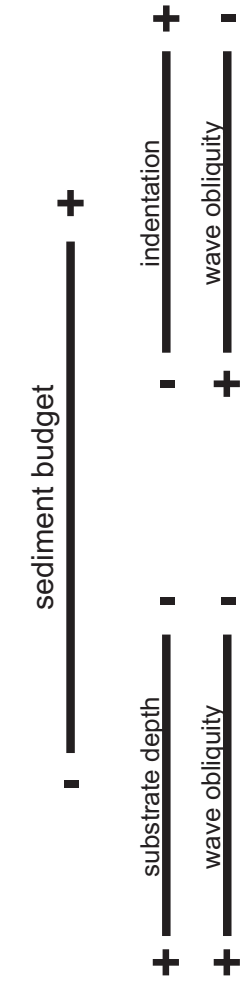

constrained process	boundary effect	morphological impact
nearshore 3D circulation	lateral	rip and bar development
longshore sediment transport	lateral	beach rotation
cross-shore sediment transport	vertical	reduced profile fluctuation
longshore sediment transport	lateral	beach rotation

Table 1

Summary of the relevant characteristics of the monitoring sites and correlation criteria

Dataset	Embayment dimensions			Sediment data		Beach profiles		Correlation criteria		
	S_l (m)	C_l (m)	B_l (m)	d_{50} (mm)	W_s (m/s)	Spacing (m)	Surveys	*DOF*	$R_{crit\ 95\%}$	$R_{crit\ 99\%}$
Amoreira	815	575	600	0.298	0.037	115	20	18	0.44	0.56
Mt. Clérigo	955	785	580	0.309	0.039	140	20	18	0.44	0.56
Arrifana	2055	1340	830	0.268	0.032	205	21	19	0.43	0.55
Salema	1300	1235	560	0.304	0.038	195	33	31	0.34	0.44
Boca do Rio	255	195	180	0.406	0.054	55	32	30	0.35	0.45
Cabanas Velhas	835	715	650	0.281	0.034	170	32	30	0.35	0.45

Abbreviations indicated in the text. Additionally, B_l stands for beach length.

Table 2
Percentage of the variance explained by the first two eigenfunctions at each site

Dataset	Percent of variance explained		
	$e_1(s,t)$	$e_2(s,t)$	Remaining
Amoreira	86,43%	10,93%	2,64%
Mt. Clérigo	91,41%	6,94%	1,65%
Arrifana	93,96%	4,44%	1,60%
Salema	66,66%	29,40%	3,94%
Boca do Rio	87,45%	8,48%	4,07%
Cabanas	92,10%	4,33%	3,57%

Table 3
Pearson's product moment correlation coefficient's between the temporal eigenfunctions ($c_n(t)$) for the peak D days averages of the hydrodynamic forcing parameters preceding each survey (only correlations at the 95% or higher confidence levels are presented).

Dataset	Correlation with forcing parameters									
	H_b	θ_b	T_p	H_o/L_o	E_o	P_o	Pn_o	Pl_b	Ω	δ'
Amoreira										
$c_1(t)$	--	--	--	--	--	--	-0.51 (1)	--	--	--
$c_2(t)$	0.65 (8)	--	0.68 (8)	--	0.62 (7)	0.65 (7)	--	0.48 (6)	0.52 (8)	-0.58 (8)
Mt. Clérigo										
$c_1(t)$	--	--	--	--	--	--	-0.65 (1)	--	--	--
$c_2(t)$	-0.49 (1)	--	--	--	--	--	--	--	-0.51 (1)	0.59 (1)
Arrifana										
$c_1(t)$	-0.52 (9)	--	-0.49 (24)	--	-0.54 (9)	-0.54 (9)	-0.88 (12)	0.49 (5)	-0.51 (9)	--
$c_2(t)$	--	--	--	--	--	--	--	--	--	--
Salema										
$c_1(t)$	--	--	-0.38 (15)	--	-0.40 (20)	-0.38 (11)	-0.53 (10)	--	--	--
$c_2(t)$	--	0.41 (6)	0.63 (15)	-0.41 (18)	--	0.36 (24)	0.37 (25)	0.35 (7)	--	-0.43 (15)
Boca do Rio										
$c_1(t)$	--	--	--	--	--	--	--	--	--	--
$c_2(t)$	--	0.55 (4)	0.44 (4)	-0.38 (2)	--	--	--	0.55 (3)	-0.35 (2)	--
Cabanas										
$c_1(t)$	-0.35 (30)	--	--	-0.36 (14)	-0.37 (29)	-0.36 (30)	-0.49 (4)	--	-0.40 (19)	0.37 (17)
$c_2(t)$	0.37 (17)	--	--	--	0.36 (18)	0.37 (17)	--	--	0.37 (17)	--

Values between parentheses indicate the averaged D days preceding each survey when the first peak in the correlation was observed. Highlighted values identify correlations exceeding the 99% confidence level. All symbols and abbreviations indicated in the text.